Prominence of ichnologically influenced macroporosity in the karst Biscayne aquifer: Stratiform "super-K" zones

Kevin J. Cunningham*
U.S. Geological Survey, 3110 SW 9th Avenue, Fort Lauderdale, Florida 33315, USA

Michael C. Sukop
Haibo Huang
Pedro F. Alvarez†
Department of Earth Sciences, Florida International University, Miami, Florida 33199, USA

H. Allen Curran
Department of Geology, Smith College, Northampton, Massachusetts 01063, USA

Robert A. Renken
Joann F. Dixon
U.S. Geological Survey, 3110 SW 9th Avenue, Fort Lauderdale, Florida 33315, USA

ABSTRACT

A combination of cyclostratigraphic, ichnologic, and borehole geophysical analyses of continuous core holes; tracer-test analyses; and lattice Boltzmann flow simulations was used to quantify biogenic macroporosity and permeability of the Biscayne aquifer, southeastern Florida. Biogenic macroporosity largely manifests as: (1) ichnogenic macroporosity primarily related to postdepositional burrowing activity by callianassid shrimp and fossilization of components of their complex burrow systems (*Ophiomorpha*); and (2) biomoldic macroporosity originating from dissolution of fossil hard parts, principally mollusk shells. *Ophiomorpha*-dominated ichnofabric provides the greatest contribution to hydrologic characteristics in the Biscayne aquifer in a 345 km² study area. Stratiform tabular-shaped units of thalassinidean-associated macroporosity are commonly confined to the lower part of upward-shallowing high-frequency cycles, throughout aggradational cycles, and, in one case, they stack vertically within the lower part of a high-frequency cycle set. Broad continuity of many of the macroporous units concentrates groundwater flow in extremely permeable passageways, thus making the aquifer vulnerable to long-distance transport of contaminants. Ichnogenic macroporosity represents an alternative pathway for concentrated groundwater flow that differs considerably from standard karst flow-system paradigms, which describe groundwater movement through fractures and cavernous dissolution features.

Permeabilities were calculated using lattice Boltzmann methods (LBMs) applied to computer renderings assembled from X-ray computed tomography scans of various biogenic macroporous limestone samples. The highest simulated LBM permeabilities were about five orders of magnitude greater than standard laboratory measurements using air-permeability methods, which are limited in their application to extremely permeable macroporous rock samples. Based on their close conformance to analytical solutions for pipe flow, LBMs offer a new means of obtaining accurate permeability values for such materials.

We suggest that the stratiform ichnogenic groundwater flow zones have permeabilities even more extreme (~2–5 orders of magnitude higher) than the Jurassic "super-K" zones of the giant Ghawar oil field. The flow zones of the Pleistocene Biscayne aquifer provide examples of ichnogenic macroporosity for comparative analysis of origin and evolution in other carbonate aquifers, as well as petroleum reservoirs.

*E-mail: kcunning@usgs.gov
†Present address: 13252 S.W. 52nd Terrace, Miami, Florida 33175, USA.

Keywords: carbonate sedimentology, ichnology, karst, lattice Boltzmann methods, aquifers, petroleum reservoirs

INTRODUCTION

Carbonate karst has been subdivided into either eogenetic or telogenetic types (Vacher and Mylroie, 2002) based on Choquette and Pray's (1970) conceptualization of the time and place that carbonate porosity is created or modified. Eogenetic karst forms during the time after final deposition and prior to burial of the sediment or rock outside the influence of near-surface meteoric diagenesis. Telogenetic karst develops in connection with unconformities during the time when long-buried carbonate rocks are exhumed following tectonic uplift. Uplifted rocks then are subjected to diagenesis by surface-related meteoric processes (Choquette and Pray, 1970; Vacher and Mylroie, 2002).

Eogenetic karst was characterized by Vacher and Mylroie (2002) as a dual-porosity system consisting of many small channels, tubes, and diverse irregular passageways organized within a matrix dominated by considerable interparticle porosity. The passageways transmit the fluids in eogenetic karst, and the interparticle porosity of the matrix provides for the storage. Fractures and caves in eogenetic karst are generally not important to regional groundwater flow (Vacher and Mylroie, 2002). Common examples of telogenetic karst include solution-enlarged conduits

GSA Bulletin; January/February 2009; v. 121; no. 1/2; p. 164–180; doi: 10.1130/B26392.1; 15 figures; 1 table; Data Repository item 2008142.

and fractures that cut across stratigraphic boundaries, where groundwater flows from sinkholes to springs (White, 1988; Ford and Williams, 1989). Telogenetic karst has been described as a dual-porosity system where the conduit and fracture porosity are most important to groundwater flow and storage, and the porosity of the matrix is essentially not notable (White, 1999). However, where matrix porosity is considered important to storage, then telogenetic karst has been characterized as a triple-porosity system (Worthington et al., 2000).

For the karst carbonate Biscayne aquifer of southeastern Florida (Fig. 1), we propose a more detailed alternative to the evolving eogenetic karst paradigm by incorporating results of examinations of outcrops and cores, carbonate cyclostratigraphy, ichnology, borehole geophysics, tracers (Cunningham et al., 2004b, 2006a, 2006b; Renken et al., 2005, 2008), and lattice Boltzmann methods (LBMs). Our karst aquifer conceptualization and its hydraulic importance were developed for a 345 km^2 main study area (Fig. 1). The Biscayne aquifer karst porosity system includes mostly Pleistocene shallow-marine platform carbonate rocks (Fig. 2). We suggest that a substantial amount of the groundwater flow in this aquifer occurs through biogenic touching-vug macroporosity (Fig. 3) that forms tabular-shaped stratiform flow zones constrained

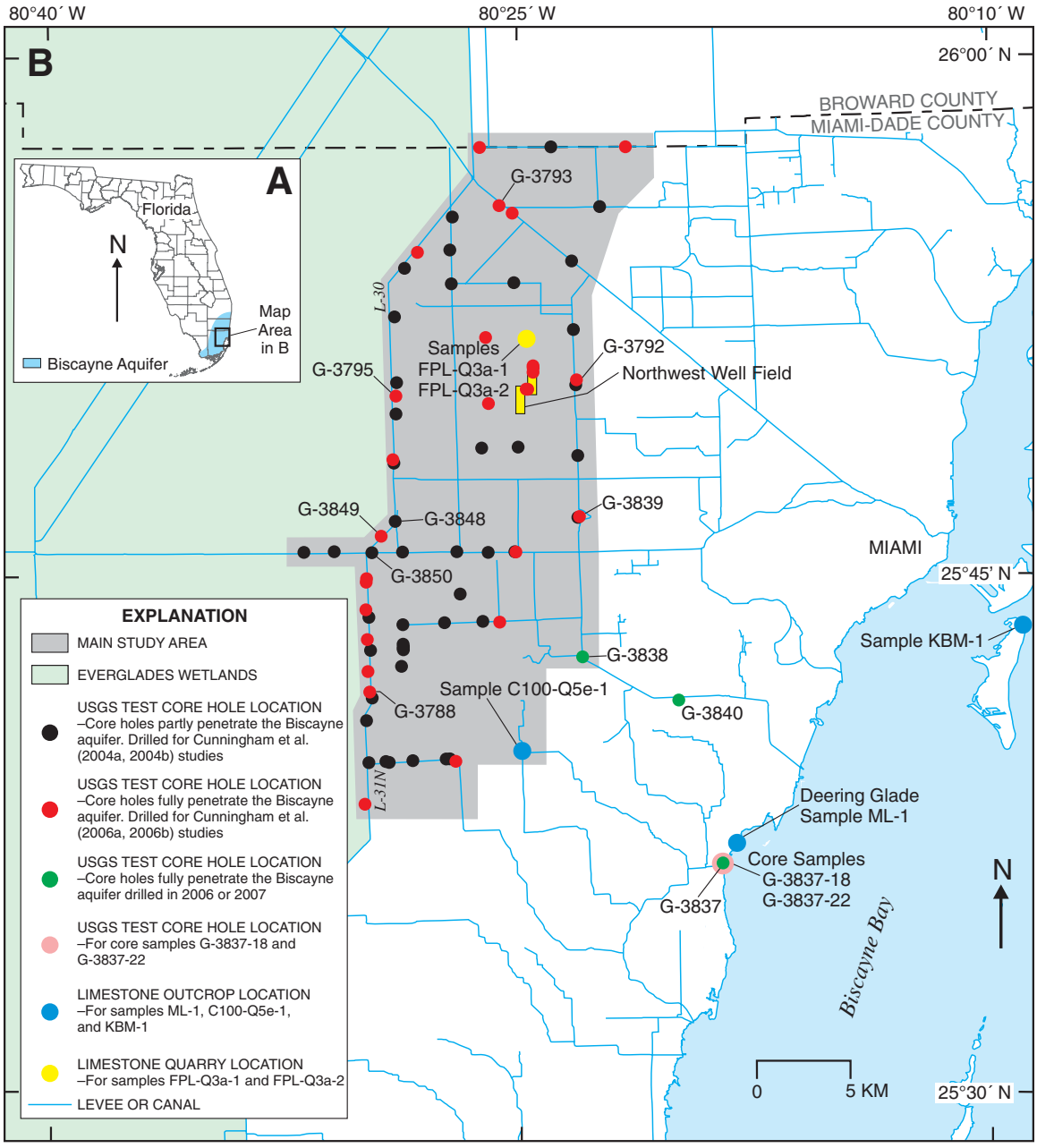

Figure 1. Study area location maps in Florida, USA. (A) Location map of area delimited in part B and areal extent of Biscayne aquifer. (B) Location of study area in southeastern Florida. Locations where lattice Boltzmann samples were collected from outcrops and test core holes are indicated.

by upper and lower bounding surfaces of high-frequency cycles. The macroporosity is commonly sandwiched between carbonate rocks dominated by matrix porosity that has characteristically interparticle and moldic pore space (Fig. 3). The biogenic macroporosity (readily visible without magnification) typically manifests as one or more of the following: inter- and intraburrow macroporosity, inter- and intraroot macroporosity, and fossil-moldic macroporosity (Fig. 3). We define ichnogenic macroporosity, a subset of biogenic macroporosity, as macropore types associated with inter- and intraburrow and inter- and intraroot macroporosity (Fig. 3). Much of the ichnogenic macroporosity of the Biscayne aquifer is related to ichnofabrics dominated by the trace fossil *Ophiomorpha*, originally created by the burrowing activity of callianassid shrimp.

The eogenetic karst limestone of the Biscayne aquifer—one of the most permeable aquifers in the world (Parker et al., 1955)—has many classic karst features variously distributed in southeastern Florida. These karst elements include: (1) small caves (Cressler, 1993); (2) subtle, relatively low-relief sinkholes, (3) large solution holes open to the surface (similar to banana holes [sensu Harris et al., 1995]), (4) vertical solution pipes, and (5) jagged rock pinnacles (Parker et al., 1955). This more classical view of the karst features of the limestone of the Biscayne aquifer was updated by Cunningham et al. (2006a, 2006b), who used data from numerous test core holes (main study area shown in Fig. 1) and reported that macroporosity associated with burrows was important to groundwater flow in the Biscayne aquifer.

Karst hydrology characterization and flow modeling are problematic due largely to a huge range in scales of hydrologic properties within karst aquifers (Whitaker and Smart, 2000). Further, the permeability of macroporous karst limestone samples is extremely difficult to measure in a laboratory setting due to flow-rate limitations of the measuring apparatus (Collins, 1952) and issues related to maintaining and measuring the extremely small gradients needed to sustain Darcian flow regimes. Our study shows that the combined use of computer renderings based on tomographic scans of decimeter-scale karst limestone samples and LBMs (Sukop and Thorne, 2006) should be considered as an alternative to

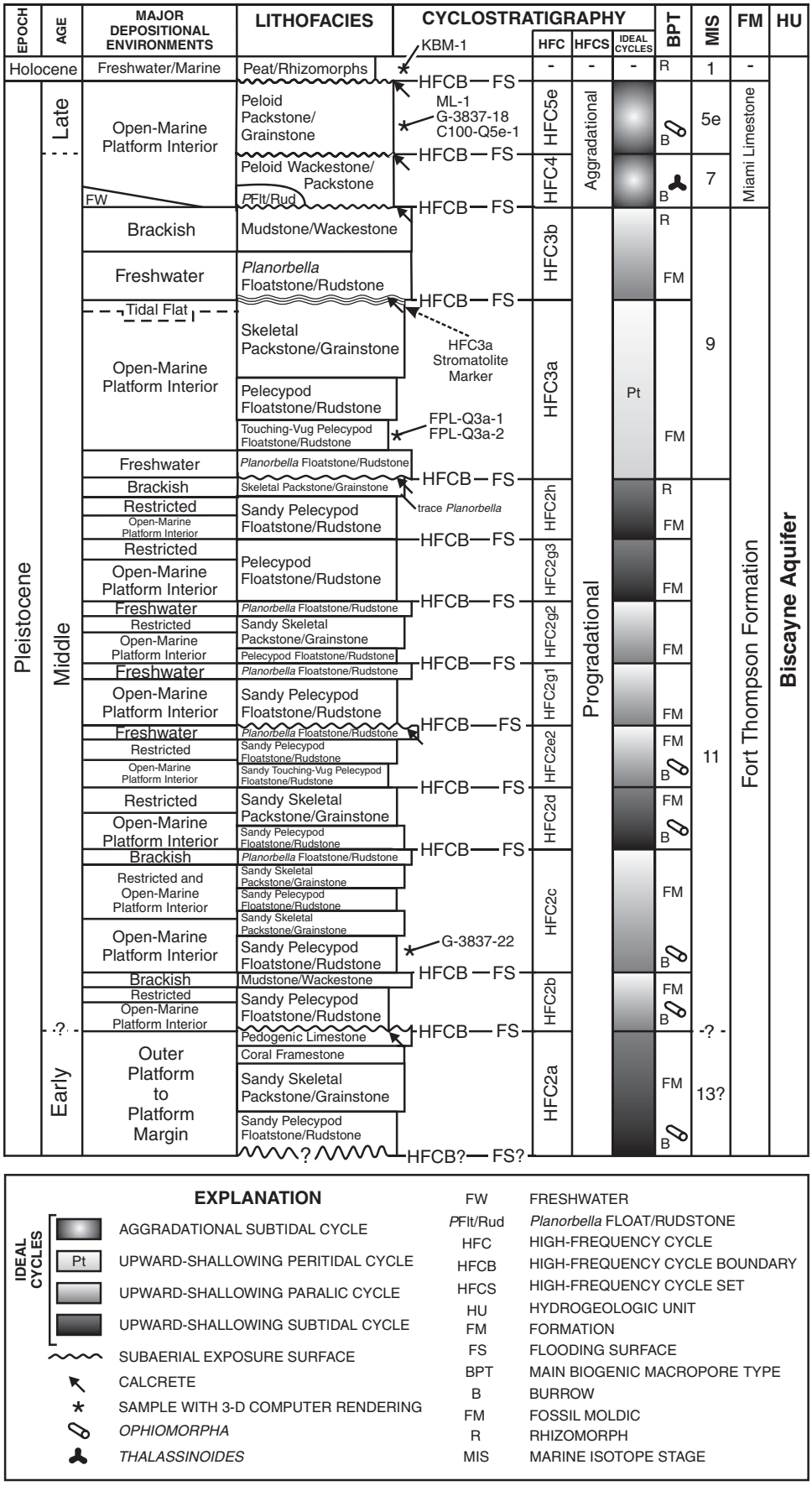

Figure 2. Conceptual hydrogeologic column of the principal lithostratigraphic and cyclostratigraphic units of the Biscayne aquifer for the main study area (Fig. 1). Figure is modified after Cunningham et al. (2006a, 2006b).

CARBONATE EOGENETIC POROSITY OF THE BISCAYNE AQUIFER					
Matrix Porosity			Touching-Vug Porosity (Vug-to-Vug Connection)		
Interparticle Porosity	Separate-Vug Porosity (Vug-to-Matrix-to-Vug Connection)		Nonbiogenic Macroporosity		Biogenic Macroporosity
	Grain Dominated	Mud Dominated	Crosscuts Strata	Stratiform	Mainly Stratiform
	Biogenic Fossil-moldic Pelmoldic Shelter Micro-ichnogenic Burrows Rhizomorphs Borings Intraparticle Nonbiogenic Oomoldic	Biogenic Fossil-moldic Pelmoldic Shelter Micro-ichnogenic Burrows Rhizomorphs Borings Intraparticle Nonbiogenic Oomoldic	Solution pipes Irregular vugs Cavernous vugs Fractures, fissures, and cracks	Bedding planes Breccia	Fossil moldic Inter- Intra- Ichnogenic Burrows Inter- Intra- Rhizomorphs Inter- Intra- Borings Growth framework Interlamination (algal)
Commonly not or poorly visible without magnification, but can be. Especially molluscan fossil-moldic porosity is readily visible without magnification			Readily visible without magnification		

Figure 3. Porosity scheme for the rocks of the Biscayne aquifer based on modification of Lucia's (1995) rock-fabric petrophysical classification of carbonate pore space. This paper focuses on those types of macroporosity highlighted in gray.

traditional bench-top methods for the measurement of extreme permeabilities of representative centimeter-scale biogenic macropore types. The main goals of this paper are (1) to describe more fully the ichnologic aspects of the macroporosity of limestones of the Biscayne aquifer in the context of a cyclostratigraphic framework and to show, more precisely than previously presented by Cunningham et al. (2006a, 2006b) and Renken et al. (2005), how this macroporosity is related to groundwater flow; and (2) to quantify, for the first time, the hydraulic conductivity of four common Biscayne aquifer biogenic macropore types (inter- and intraburrow macroporosity, fossil-moldic macroporosity, and interroot macroporosity) using intrinsic permeability values calculated from LBMs.

BACKGROUND

Hydrogeology and Cyclostratigraphy of the Limestone of the Biscayne Aquifer

The current physical setting for the unconfined, sole-source Biscayne aquifer is a low-elevation, subtropical environment. The rocks and sediment that define the top of the Biscayne aquifer are exposed at the ground surface—their areal extent, which corresponds to the geographic limits of the Biscayne aquifer, is shown in Figure 1A. In the map area of Figure 1B, the depth below sea level of the base of the Biscayne aquifer ranges between ~6 and 57 m and generally dips eastward. The main lithostratigraphic units of the Biscayne aquifer are the Fort Thompson Formation and Miami Limestone (Fig. 2), both of which are characterized by eogenetic karst limestone (Cunningham, 2004b, 2006a, 2006b). These carbonate units were deposited mostly in shallow, subtropical- to tropical-marine shelf or continental-marine transitional environments. The limestone was not subject to deep burial, and multiple widespread subaerial discontinuities associated with sea-level lowstands are interspersed throughout the limestone system (Perkins, 1977; Multer et al., 2002); thus, the limestone commonly has substantial primary interparticle and secondary moldic porosity. We describe the Biscayne aquifer as a dual-porosity pore system (cf. Cunningham et al., 2004b, 2006a, 2006b), consisting of a (1) matrix (interparticle and separate vugs) porosity, which provides much of the groundwater storage, and (2) touching-vug macroporosity (biogenic macroporosity), which creates stratiform, areally extensive, groundwater flow pathways and less common bedding-plane and cavernous vugs, and thin, vertical solution pipes (Fig. 3). The geology and hydrology of the Biscayne aquifer have been reported in numerous studies (Parker et al., 1955; Perkins, 1977; Fish and Stewart, 1991; Galli, 1991; Cunningham et al., 2004b, 2006a, 2006b; Renken et al., 2005). The cyclostratigraphy of the Miami Limestone and Fort Thompson Formation (Fig. 2) was described in detail by Cunningham et al. (2006a, 2006b), who recognized three ideal high-frequency cycle types. We include a fourth ideal high-frequency cycle type (Figs. 2 and 4)—an upward-shallowing peritidal cycle, which is unique in its occurrence to marine isotope stage (MIS) 9.

Ichnology of the Miami Limestone and Fort Thompson Formation

In southeastern Florida, the general ichnological characteristics of the high-frequency cycle of the Miami Limestone assigned to MIS 5e (Fig. 2) have been studied and documented by Perkins (1977), Halley and Evans (1983), Evans (1984), and Evans and Ginsburg (1987). Earlier, Shinn (1968) documented "cone-in-cone structure" (*Conichnus conicus*) in the Miami Limestone and postulated an origin related to the upward-burrowing activity of sea anemones. Curran (2007) devised an ichnocoenoses model for the *Skolithos* and *Psilonichnus* ichnofacies of the Bahamas and applied it to the high-frequency cycle of the Miami Limestone correlated to MIS 5e.

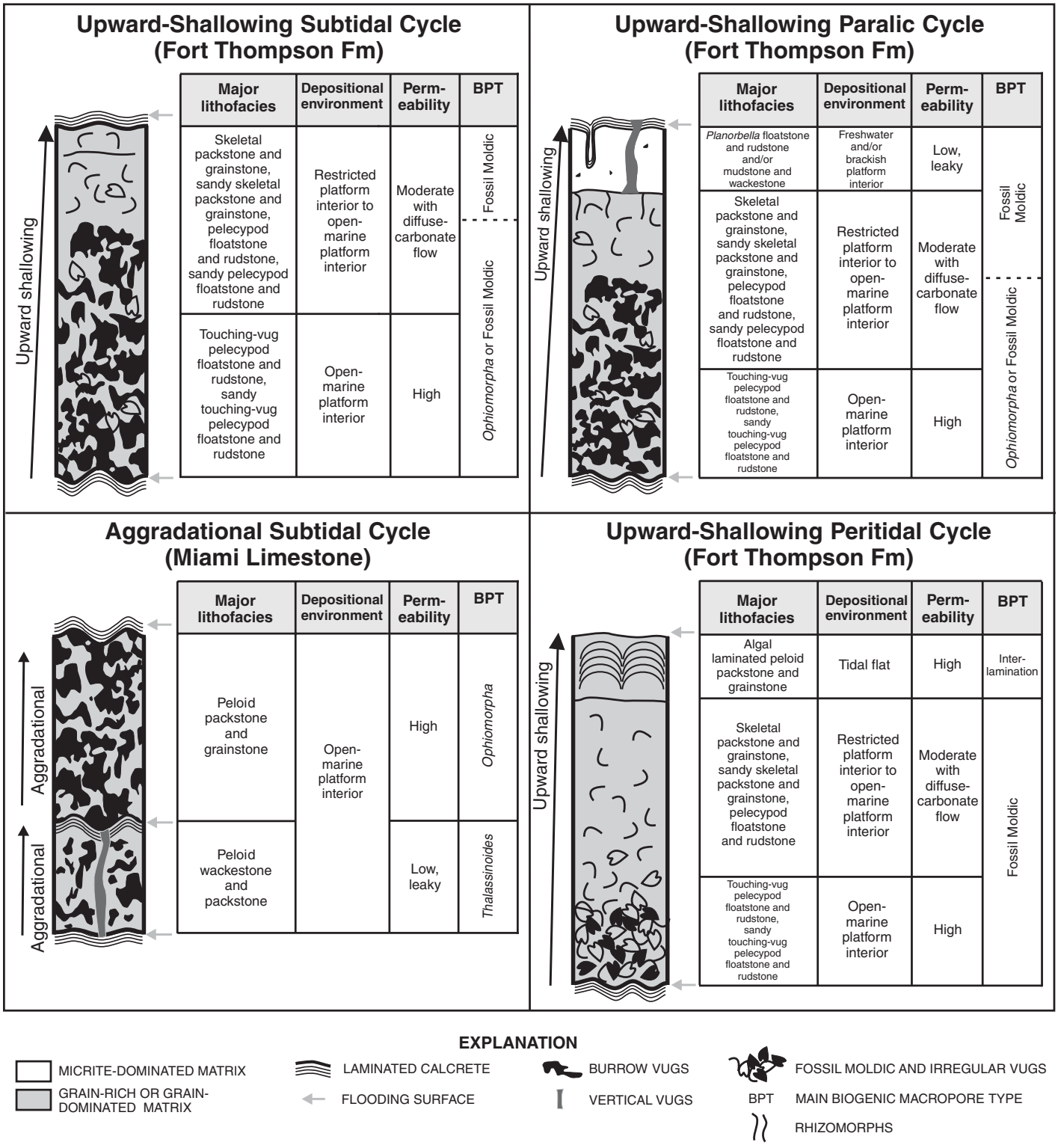

Figure 4. Idealized high-frequency cycles for the Fort Thompson Formation and Miami Limestone showing relations among lithofacies, depositional environments, permeability, and biogenic macroporosity. Figure is modified after Cunningham et al. (2006a, 2006b).

METHODS

Methods used to characterize the pore system of the Biscayne aquifer included integrating data from new and/or existing geologic (including cyclostratigraphy and ichnology) and hydraulic analyses of outcrops and cores, borehole-geophysical logs, tracer studies, high-resolution X-ray computed tomography (HRXCT) scans of seven limestone samples, macroporosity measurements from volume renderings, and lattice Boltzmann measurements of intrinsic permeability. For details of methods related to sample examination, cyclostratigraphy, drilling, borehole-geophysical and borehole–flow meter measurements, and tracer studies, refer to Cunningham et al. (2004a, 2004b, 2006a, 2006b) and Renken et al. (2005).

Laboratory Measurement of Porosity and Permeability for Whole Cores

Four full-diameter (10.16 cm) limestone core samples from the Miami Limestone and Fort Thompson Formation were measured at Core Laboratories, Inc., for porosity and permeability. For comparison of methods, calculation of macroporosity and LBM measurement of intrinsic permeability were later conducted on computer renderings of the samples. Laboratory porosity was determined using a helium pycnometer. The core samples were measured (using air flow) for permeability in two horizontal directions and one vertical direction while in a Hassler rubber sleeve. The permeameter methodology used by the laboratory is based on Collins (1952). The highest range of accurate permeability values measured using this routine method is between 10 and 30 Darcies (J. Dacy, 2007, personal commun.) or, converted to hydraulic conductivity, ~0.0001 m/s and 0.0003 m/s, respectively.

High-Resolution X-Ray Computed Tomography (HRXCT), Three-Dimensional (3-D) Computer Renderings, and Macroporosity Calculations

The High-Resolution X-Ray CT Facility at the University of Texas at Austin performed HRXCT scans (Ketcham and Carlson, 2001) on seven macroporous Biscayne aquifer limestone samples (Table DR1[1]) collected from Holocene limestone, Miami Limestone, and Fort Thompson Formation (Fig. 2). Individual computed tomography (CT) scan images are referred to as slices. Acquisition of sample CT slices was at 0.8 mm increments and overlapped to create 1.0-mm-wide slices in computer renderings. The CT slices for each limestone sample were combined into a series of CT slices to create a 3-D RAW format file for use as an LBM input file. For example, ML-1 (Figs. 5 and 6; Table DR1 [see footnote 1]) had 401 slices made up of 1024 × 1024 pixels. The images had a resolution of 0.271 mm in length and width per pixel, which is the scaling relation for determining physical values from those produced by the model in lattice Boltzmann units.

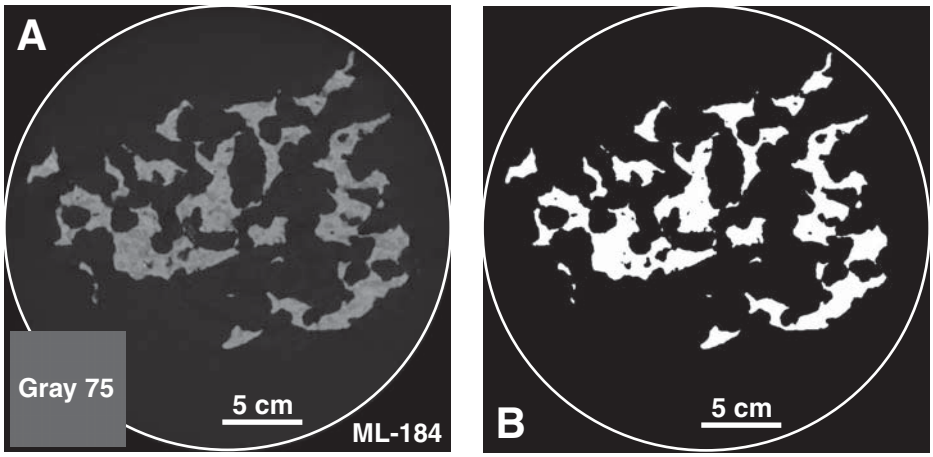

Figure 5. High-resolution X-ray computed tomography scan images through limestone specimen ML-1 (Fig. 1 and Table DR1 [see text footnote 1]). (A) Image of scan (ML-184) before conversion into the black and white image in (B). Lighter-gray areas are limestone matrix (peloid, ooid grain-dominated packstone to grainstone), and very dark gray areas are pore space. (B) Scan showing limestone matrix as white and pore space as black. The gray level (75) used for threshold is shown in (A).

The original slices were in 8 bit jpg formats with grayscale values ranging from 0 to 255. A threshold grayscale value of 75 was selected because it best differentiated between macropores and solids and produced binary images, where the color black was assigned to the areas indicated as macropores and white was assigned to the rock matrix (Fig. 5). Mostly porous but relatively low-permeability rock matrix therefore was rendered as a nonporous and impermeable solid in the context of the LBMs. However, given a much larger size for macropores as compared to substantially smaller pores within the rock matrix (Fig. 5),

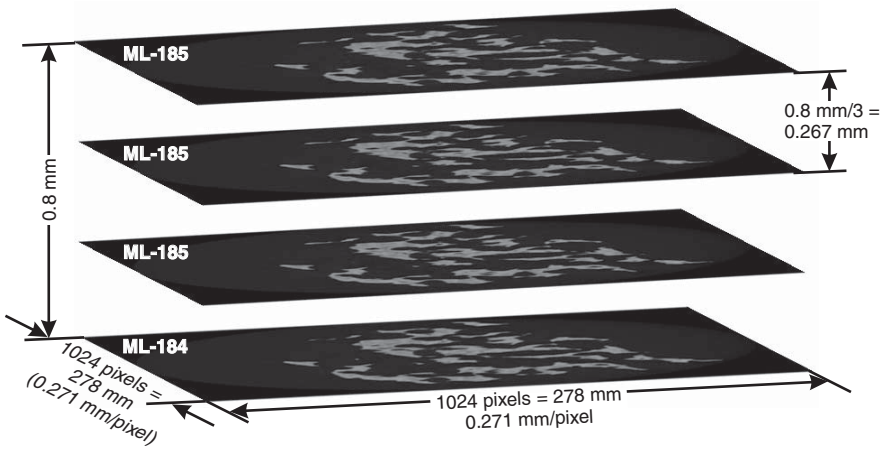

Figure 6. Interpolation between high-resolution X-ray computed-tomography scan images based on three repetitions of slice ML-185. The resulting *z*-spacing is 0.267 mm, while the pixel spacing in the *x* and *y* directions is 0.271.

[1]GSA Data Repository Item 2008142, two tables and seven videos, is available at www.geosociety.org/pubs/ft2008.htm. Requests may also be sent to editing@geosociety.org.

this method was appropriate for the purposes of permeability measurement.

For the lattice Boltzmann reconstruction, the *z*-direction scaling of the 3-D image had to be adjusted, since the *z*-axis spacing was not the same as the *x*- and *y*-axis spacing in the CT data set (Alvarez, 2007). As noted already, the *x* and *y* spacing was 0.271 mm; however, the *z* or slice spacing was 0.8 mm (Fig. 6). In order to interpolate between the slices and obtain a virtual representation of the ML-1 rock sample, which closely approximated the physical sample and provided almost equidistant node spacing in all directions, we repeated each slice three times as depicted in Figure 6. In this way, the 0.8 mm distance between the original slices was divided into three segments with a spacing of 0.267 mm (0.8 mm/3). This is close to the *x* and *y* pixel spacing (Fig. 6). Thus, the original 401 CT slices were expanded to 1203 slices.

Following differentiation of macropores and solids by application of the grayscale threshold, expansion to obtain the correct *z*-axis scaling, and cutting of a subvolume to ensure that its boundaries lay entirely within the boundaries of each limestone sample, macroporosity was determined by pixel counting. For individual samples, macroporosity was derived as the sum of the macropore pixels found on each slice divided by the sum of macropore and solid pixels on each slice.

Lattice Boltzmann Computer Simulation

LBM is a powerful technique that can be used for computational modeling of complex fluid flow. This method was used to calculate intrinsic permeabilities of computer renderings of our seven macroporous limestone samples. The LBMs were based on statistical physics and the Navier-Stokes equations for fluid flow (Sukop and Thorne, 2006). The LBMs that we employed to calculate intrinsic permeability have been summarized in Alvarez (2007). Detailed information regarding the LBMs can be found in Succi (2001) and Sukop and Thorne (2006).

ICHNOLOGY, CYCLOSTRATIGRAPHY, AND GROUNDWATER FLOW IN THE BISCAYNE AQUIFER

General

Structures produced by burrowing organisms can be important modifiers of sediments accumulating in subtropical to tropical shallow-marine carbonate environments (Shinn, 1968; Tedesco and Wanless, 1991; Curran and Martin, 2003; Curran, 2007). Burrowers can have a considerable impact on original sedimentary textures, fabrics, and structures—to the point of total transformation of precursor depositional units and creation of new sedimentary deposits (e.g., Tedesco and Wanless, 1991). The principal burrowers in tropical, shallow-subtidal carbonate sand environments are thalassinidean shrimp, especially callianassids, which can occur in high densities (Curran and Martin, 2003). Southern Florida, the islands and bank tops of the Bahamas, and tropical carbonate islands elsewhere provide numerous examples of Quaternary shallow-marine carbonate rocks dominated by *Ophiomorpha* ichnofabrics generated by callianassids (Halley and Evans, 1983; Curran, 2007). As callianassid burrowing changes textures and fabrics, the sediment pore system is completely reorganized and likely enhanced by creation of numerous open shafts and tunnels. Conversely, porosity occlusion can take place with the redistribution of fine sediment as it is forced between larger grains during construction of the thick walls of extensive burrow complexes. The new, ichnogenically engineered pore system, combined with dissolutional diagenetic overprinting, can result in a carbonate rock with greatly enhanced porosity and permeability.

Biogenic Macroporosity

In the Biscayne aquifer, biogenic macroporosity mostly manifests as two forms of touching-vug macroporosity: (1) moldic macroporosity generated by the dissolution of organism hard parts, principally mollusk shells (Fig. 7A); and (2) ichnogenic macroporosity resulting primarily from callianassid burrowing activity. Figure 3 shows our classification scheme for carbonate rocks of the Biscayne aquifer based on a modification of the rock-fabric–petrophysical classification of carbonate pore space by Lucia (1995). Our definition of ichnogenic macroporosity includes intra- or interburrow macroporosity (Fig. 8) and, less commonly, intra- or inter-root macroporosity (Fig. 7B). Intraburrow macroporosity, in grain-dominated limestone, results from dense occurrences of *Ophiomorpha*, where crosscutting of burrow tunnels and shafts by multigenerational burrowing can produce a well-connected system of macroporosity (Fig. 9A). The *Ophiomorpha* tubes commonly remain open, or are later washed clean or cleared of fill via dissolution, generating intraburrow macroporosity. With dissolution, *Ophiomorpha* segments may lose part or all of the burrow lining, usually from the inside outward. Interburrow macroporosity most likely forms by transport away or dissolution of less well-lithified matrix, more permeable matrix, or a less stable mineralogy surrounding dense complexes of *Ophiomorpha*-related rigid frameworks (Fig. 8). Commonly, intra- and interburrow macroporosities occur together, creating a highly permeable rock (Fig. 8).

Common Biogenic Macroporosity Types and Cyclostratigraphy

In our main study area (Fig. 1), the occurrence of biogenic macroporosity is related to vertical stacking of lithofacies and associated depositional environments within the: (1) four idealized high-frequency cycles of the Miami Limestone and Fort Thompson Formation (Fig. 4), and (2) high-frequency cycle sets that constitute these two lithostratigraphic units (Fig. 2). Biogenic macroporosity associated with thalassinidean-produced ichnofabrics dominates the aggradational subtidal high-frequency cycles of the cycle set (MIS 5e and 7) equivalent to the Miami Limestone (Figs. 2 and 4). Fossil-moldic macroporosity dominates the upward-shallowing subtidal, paralic, and peritidal cycles of the upper part of the progradational high-frequency cycle set (MIS 9 and younger part of 11) that define the upper Fort Thompson Formation (Figs. 2 and 4). *Ophiomorpha* ichnofabric and associated macroporosity are predominant in the upward-shallowing subtidal and paralic cycles of the lower part of the progradational high-frequency cycle set (older part of MIS 11 and 13?) that correspond to the lower Fort Thompson Formation (Figs. 2 and 4).

Ophiomorpha ichnofabric and related macroporosity are predominant throughout the vertical thickness of the grain-dominated peloid packstone and grainstone that compose the high-frequency cycle correlated to MIS 5e (Fig. 2). Eastward of our main study area (Fig. 1), the high-frequency cycle assigned to MIS 5e has the greatest variety of trace fossils (Fig. 9), including *Ophiomorpha*, *Conichnus*, *Planolites*, *Skolithos*, and rhizomorphs (root traces). However, *Ophiomorpha* clearly represent the principal ichnofabric-forming trace fossil at a broad scale. The most extreme example of large-scale porosity associated with *Ophiomorpha* ichnofabric is at Deering Glade (Fig. 1), where a stratiform unit characterized by a maximum *Ophiomorpha* ichnofabric (Fig. 9A) has undergone very aggressive dissolution to form associated caves of substantial size (Cunningham et al., 2008, their Fig. 4).

A *Thalassinoides* ichnofabric is most common in mud-dominated wackestone and packstone of the high-frequency cycle of the Miami Limestone assigned to MIS 7 (Figs. 2, 4, and 9B), but, in contrast to highly macroporous lithofacies containing a maximum *Ophiomorpha* ichnofabric, it is characterized by relatively low macroporosity. The upper walls of

Thalassinoides shafts and tunnels are commonly lined with secondary pendant calcite cement (Fig. 10), and the remaining burrows are filled with an allochthonous fine sediment, commonly quartz sand-rich peloid grainstone or quartz sand (Fig. 9B). Thus, much of the original intraburrow porosity is occluded.

In the lower part of the Fort Thompson Formation (Fig. 2), dense concentrations of *Ophiomorpha* are generally constrained to grain-dominated limestone in the lower part of upward-shallowing subtidal and paralic high-frequency cycles (Figs. 2 and 4) and are generally associated with an open-marine platform interior depositional environment. Importantly, in the Fort Thompson Formation, a concentration of vertically stacked *Ophiomorpha*-related macroporous zones in the lower part of the upward-shallowing progradational high-frequency cycle set mimics the common occurrence of the same macroporosity type in the lower part of upward-shallowing high-frequency cycles (Fig. 2). Thus, in the Fort Thompson Formation, *Ophiomorpha*-associated macroporosity is commonly found in the lower part of upward-shallowing cyclicity at two scales, and this type of macroporosity is concentrated in that part of the high-frequency cycles and the cycle set where the deepest paleodepth is interpreted.

The most robust vertical stack of high-frequency cycles dominated by *Ophiomorpha* ichnofabric occurs in the western part of the main study area (Fig. 1). Digital optical borehole images at cored monitoring well G-3849 (Fig. 1) show that *Ophiomorpha* ichnofabric and related macroporosity are major features within the high-frequency cycles assigned to MIS 5e, 9, and 11. The ichnogenic macroporosity is present in up to 77% of the vertical thickness of the limestone of the Biscayne aquifer (Fig. 11). This example demonstrates the huge impact that *Ophiomorpha* ichnofabric can have on the heterogeneity of macroporosity in the Biscayne aquifer.

Groundwater Flow

In the main study area (Fig. 1), results from: (1) borehole-fluid flow measurements, (2) tracer studies at a municipal well field, and (3) permeabilities derived from LBMs indicate that ichnogenic macroporosity is an important contributor or even dominates the groundwater flow system of the Biscayne aquifer.

Borehole-Fluid Flow Measurements

Identification of vertical borehole flow was utilized to test the hypothesis that biogenic macroporosity is responsible for most of the

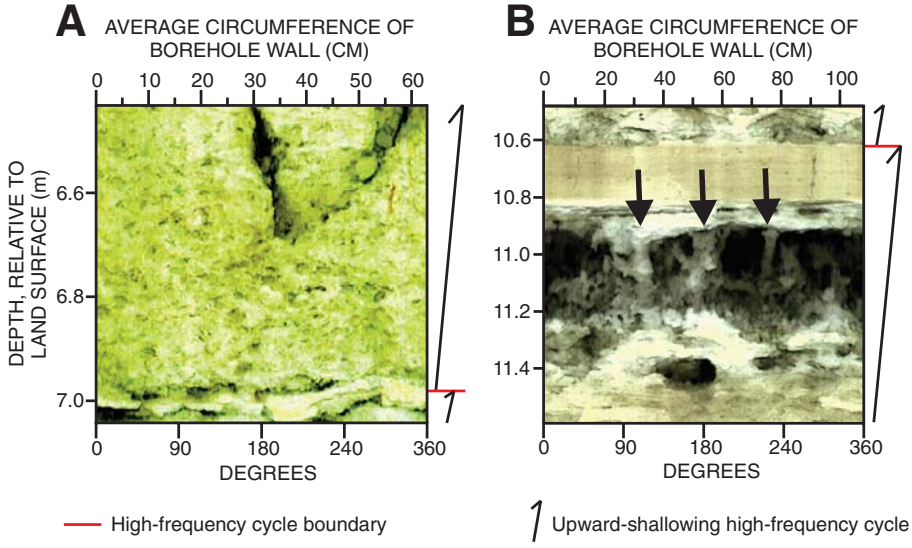

Figure 7. Digital images of borehole walls. (A) Fossil-mold macroporosity due to dissolution of mainly pelecypod shells near the base of high-frequency cycle 3a of the Fort Thompson Formation, which overlies a thin, laminated calcrete at the top of high-frequency cycle 2h (Fig. 2). Image is from test core hole G-3792 (Fig. 1). (B) Root casts or rhizomorphs (arrows), probably mangrove, and inter-root macroporosity beneath a cycle-capping lime mudstone deposited in a brackish-water paralic environment during marine isotope stage 11 (MIS 11). Image is from test core hole G-3795 (Fig. 1).

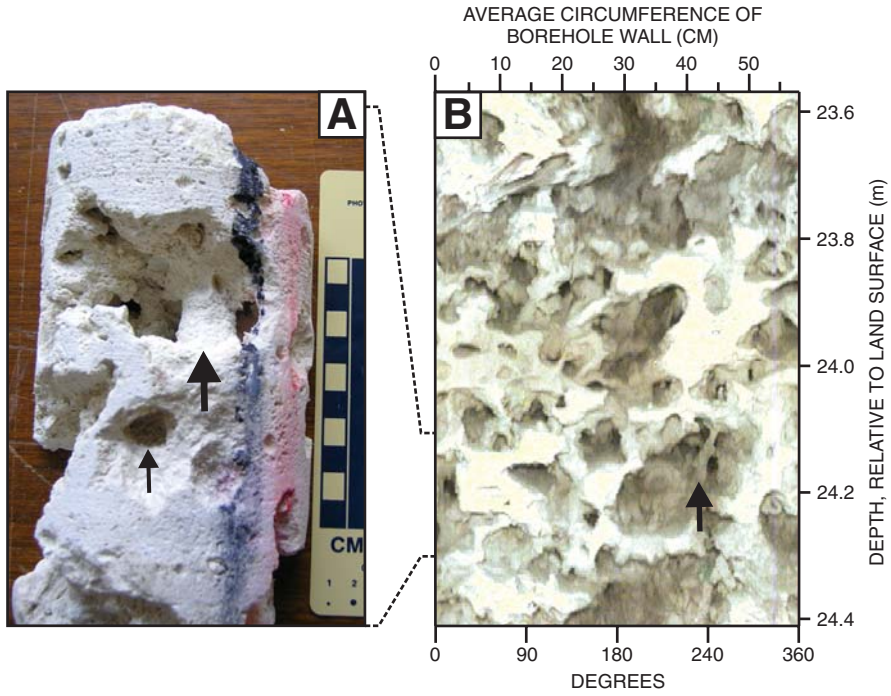

Figure 8. Substantial interburrow porosity from the marine isotope stage 11 part of test core hole G-3839 (Fig. 1). (A) Core sample from depth of 24.1–24.3 m. Large arrow points to *Ophiomorpha* shaft with an ~2 cm outer diameter, about a 2.3 cm length, surrounded by interburrow porosity. Small arrow indicates interior of probable *Ophiomorpha* shaft with an ~2 cm inner diameter. (B) Digital optical borehole image from ~23.6–24.4 m. Arrow points to probable *Ophiomorpha* shaft with about a 1.8 cm outer diameter, ~8 cm length, surrounded by interburrow porosity.

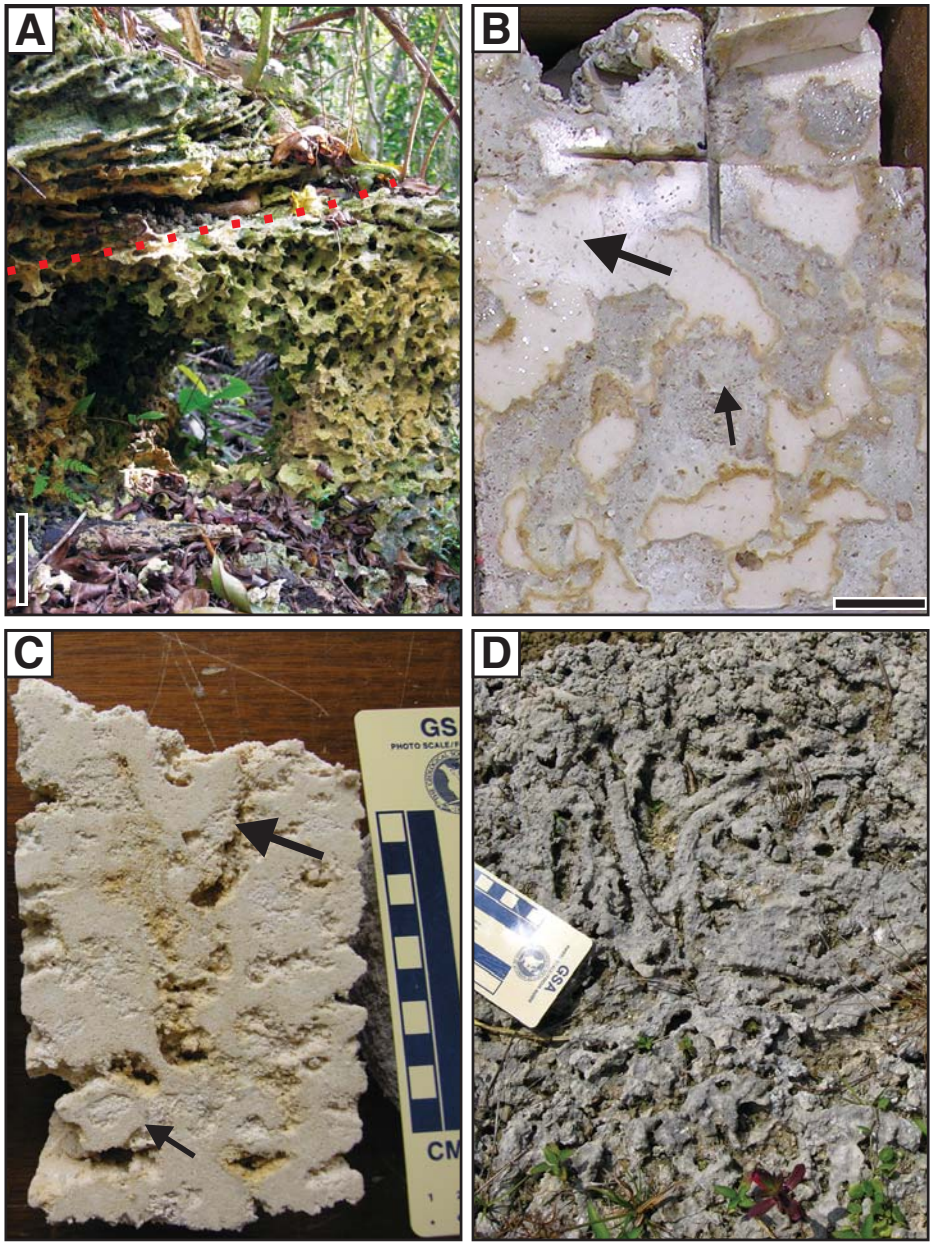

Figure 9. Major ichnofabrics of the Miami Limestone for area shown in Figure 1B. (A) Miami Limestone (marine isotope stage [MIS] 5e) outcrop at Deering Glade where sample ML-1 was collected (Tables 1 and DR1 [see text footnote 1]) within barrier-bar environment of Halley et al. (1977). Below red dashed line is maximum intensity *Ophiomorpha* ichnofabric and ichnoporosity in a peloid, ooid grain-dominated packstone to grainstone matrix. Above is downlapping, cross-laminated oolite. Caves are common within the *Ophiomorpha*-rich unit. Bar scale = 10 cm. (B) Low-permeability MIS 7 sample from a lagoonal or shallow-shelf environment showing maximum intensity *Thalassinoides* ichnofabric with allochthonous quartz-sand–rich, grain-dominated packstone filling irregular tunnels and shafts (small arrow) constructed by non-callianassid thalassinidean shrimp, possibly upogebiids, in a micrite-rich matrix (large arrow). Core sample is from test core hole G-3838 (Fig. 1) at 5.4 m below the surface. Bar scale = 2 cm. (C) Slabbed core (MIS 5e) acquired from a tidal-channel environment with *Conichnus conicus* (large arrow) and *Ophiomorpha* (small arrow) specimens. Core sample is from test core hole G-3840 (Fig. 1) at 3.7 m below the surface. (D) MIS 5e outcrop with abundant *Planolites* parallel with bedding from a tidal-channel environment.

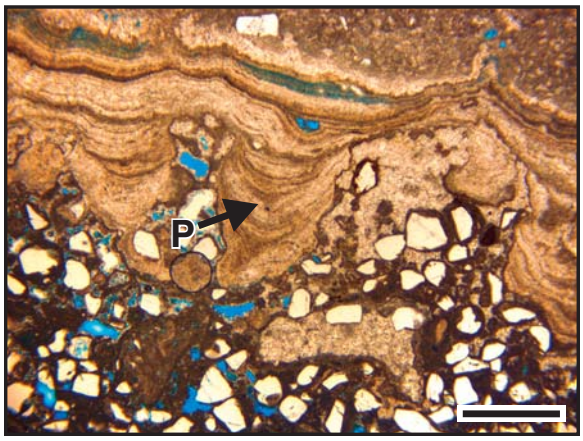

Figure 10. Thin-section photomicrograph in plain light of core sample showing pendant calcite cements in *Thalassinoides* burrow from the high-frequency cycle of the Miami Limestone assigned to marine isotope stage 7 in test core hole G-3838 (G-3838–17.21; Fig. 1) at a depth of 5.2 m below the surface. P—pendant cement; black bar scale = 1.0 mm.

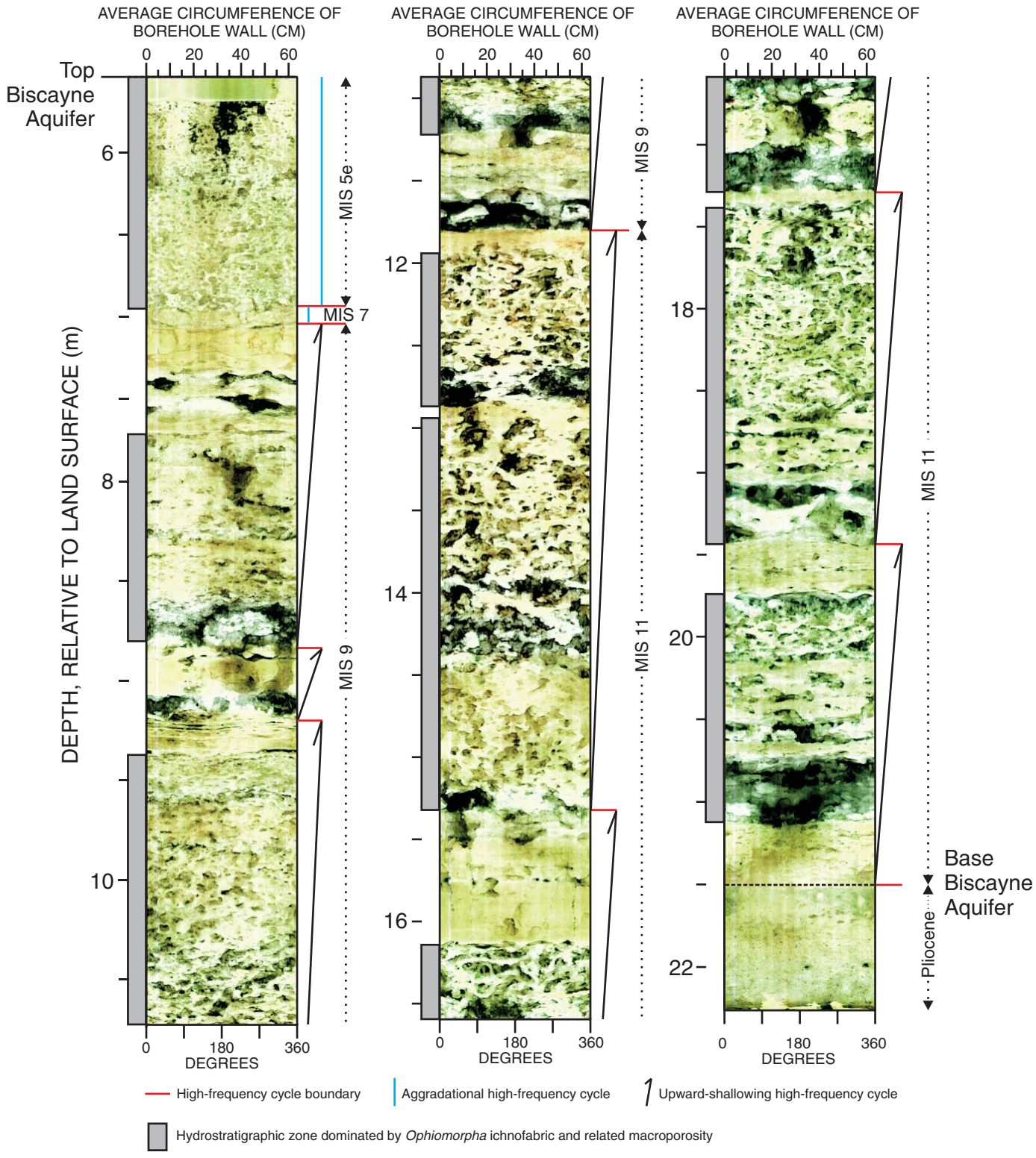

Figure 11. Digital optical logs from the G-3849 test core hole (Fig. 1) showing maximum *Ophiomorpha* ichnofabric and related inter- and intraburrow macroporosity throughout the vertical thickness of the Biscayne aquifer. The zones of ichnoporosity make up 77% of the vertical thickness of the limestone composing the Biscayne aquifer.

groundwater flow in the Biscayne aquifer within the main study area (Fig. 1). Borehole-fluid flow was detected in conjunction with the acquisition of borehole–flow meter, fluid-conductivity, fluid-temperature (Table DR2 [see footnote 1]), and digital borehole image data. For log measurements within the Biscayne aquifer (Table DR2 [see footnote 1]), borehole-fluid temperature ranged from 22.0 to 31.6 °C, and borehole-fluid conductivity ranged from 336 to 807 µS/cm. Intervals of the borehole where water inflow or outflow were identified (Fig. 12) showed substantial shifts in values of vertical borehole flow, fluid conductivity, and fluid temperature over a short vertical distance (Fig. 12). Identification of other flow intervals was based on only one or two of these parameters. These flow zones mostly occurred at the base of high-frequency cycles (Table DR2 [see footnote 1]). Geophysical measurements across 64 flow zones in 16 boreholes indicate that biogenic porosity is the principal pore type in groundwater flow zones, and ichnogenic macroporosity is important in most. Bedding-plane vugs or irregular vugs were found to be subordinate contributors to flow zones and only a single cavernous-sized flow zone was identified.

Two preferential flow zones that are dominated by biogenic macroporosity are present in the upper part of the Biscayne aquifer throughout the main study area. These zones include all of the high-frequency cycle assigned to MIS 5e and the lower part of the high-frequency cycle correlated to the older part of MIS 9 (Cunningham et al., 2006b, their Fig. 32). The high-frequency cycle correlated to MIS 5e corresponds to the regionally mapped Q5 unit of Perkins (1977), which he correlated over a large area in Miami-Dade County. In addition, a fossil-moldic macroporosity zone assigned to the older part of MIS 9 has been correlated (Cunningham, 2006b) well beyond our main study area (Fig. 1). Seven preferential flow zones dominated by biogenic porosity were identified as widely important in high-frequency cycles assigned to MIS 11 and 13?, and five zones were identified in the Biscayne aquifer where inflow or outflow from the borehole was delineated locally (Cunningham et al., 2006b, their Fig. 32).

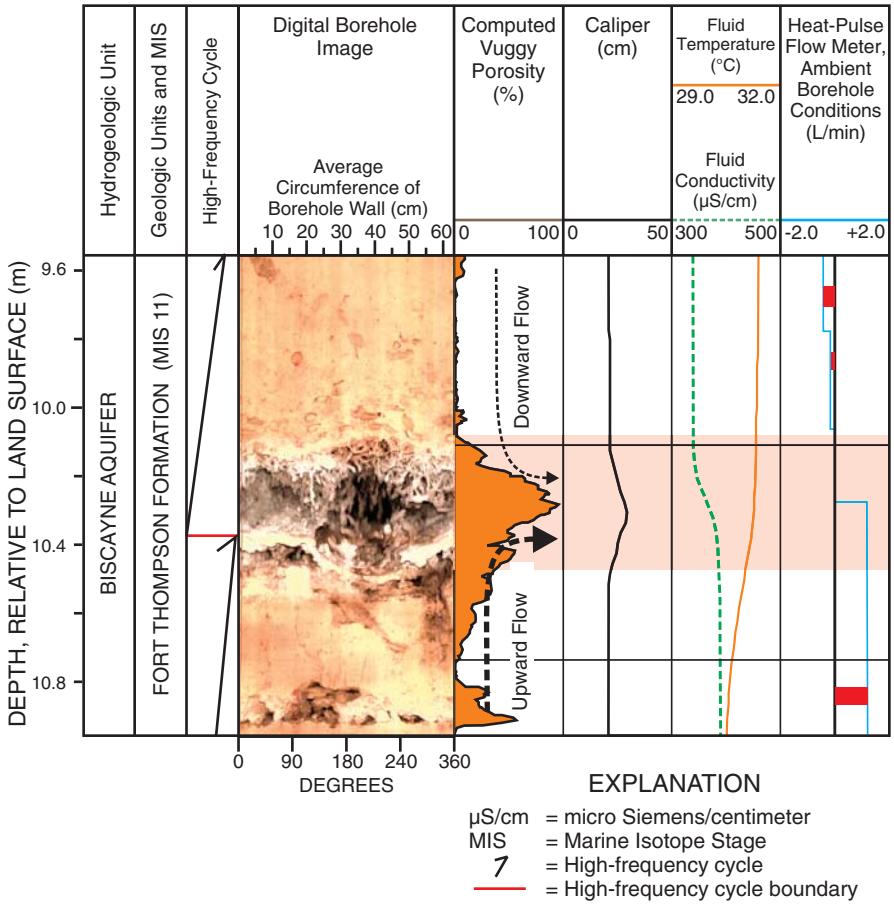

Figure 12. Comparison of borehole image, computed vuggy porosity (Cunningham et al., 2004a), geophysical, and flow meter logs showing evidence of flow of groundwater out of the borehole and into an ichnogenic macroporous preferential flow zone penetrated by the G-3788 test core hole (Fig. 1). Most of the flow out of the borehole occurs at a vuggy cavity at the base of a high-frequency cycle assigned to marine isotope stage 11 between the depths of ~10.1 and 10.5 m below land surface (zone shaded in pale red). Stringy casts in middle to upper part of vuggy cavity may be rhizomorphs.

Tracer Studies

In 2003, a forced-gradient tracer test using the conservative tracers, rhodamine WT, and deuterium, was performed in the Northwest Well Field (Fig. 1). Dominant pathways for groundwater flow and chemical transport are stratiform beds of touching-vug pore space, principally formed by intra- and interburrow macroporosity (Renken et al., 2005; Cunningham et al., 2006a). The karst limestone behaves as a dual-porosity aquifer during pumping (Renken et al., 2008). Limestone strata, characterized by matrix porosity and a lower permeability, release groundwater held in storage, supplementing flow within the highly transmissive macroporous flow zones.

Results of the tracer test and temperature logging in an observation well suggest that one of several touching-vug flow zones dominated tracer migration. That zone is principally intra- and interburrow ichnogenic macroporosity (Cunningham et al., 2006a, their Fig. 7), made up mainly of an *Ophiomorpha* ichnofabric. Tracer movement was characterized by rapid tracer pulse breakthrough (369 m/d), high relative mass recovery, and advective transport with low dispersivity (Renken et al., 2005, 2008). A dominance of tracer movement by advection strongly indicates transport along preferential flow paths within ichnogenic macroporosity.

Lattice Boltzmann Methods (LBMs) Simulations

Following procedures used for sample ML-1 (Figs. 13A, 14A, and 14D; Table DR1 [see footnote 1]), LBMs were used to obtain intrinsic permeabilities of seven samples representative of biogenic macroporosity (Figs. 13 and 14; Table 1 and Table DR1 [see footnote 1]). Although the physical ML-1 sample volume was ~27,000 cm^3, a subsample domain of ~729 cm^3 (~3.8×10^7 lu^3; Fig. 14D) was selected to ensure that the model domain was entirely within the boundaries of the sample, where one lattice unit (Δx) is defined as 1 lu. The flow simulation domain was slightly larger than the subsample domain (~4.0×10^7 lu^3) because four impermeable walls bounded it, except on top and bottom surfaces perpendicular to the z axis. Additional volume was added to the simulation domain by

adding seven slices, each containing only pore space at both the inlet and outlet end (top and bottom perpendicular to the z axis), to act as uniform pressure reservoirs and accommodate the applied pressure boundary conditions (Zou and He, 1997).

A pressure gradient was established across the simulation domain parallel to the direction of interest, and the difference between the inlet and outlet fluid mass flux was monitored. As steady-state flow was established, the difference between the inlet and outlet flows approached zero. Darcy's law has the form,

$$q = \frac{k}{\rho\nu}\frac{\Delta p}{L} = \frac{k}{\rho c_s^2(\tau - 0.5)}\frac{\Delta p}{L}, \qquad (1)$$

where q is the Darcy flux, k is the intrinsic permeability, p is the pressure, ρ is the average density, L is the length over which the pressure drop occurs, τ is the LBM relaxation time, c_s is the LBM sound speed ($1/\sqrt{3}$ lu ts^{-1}), and ν is the kinematic viscosity ($c_s^2[\tau - 0.5]$ in the LBM). Note that the average density (ρ) is used in the denominator of Equation (1). In our simulation, the average fluid density was $\rho = 1$ mu lu^{-3}, $\Delta\rho = 0.000546$ mu lu^{-3}, and inlet and outlet pressure were $p_{in} = c_s^2(1 + \Delta\rho)$ and $p_{out} = c_s^2(1 - \Delta\rho)$ mu lu^{-1} ts^{-2}, respectively, according to the Equation (2),

$$p = c_s^2\rho, \qquad (2)$$

which is an equation of state. It relates the pressure and density in the LBM that is applied when defining pressure boundaries in simulations. The summed velocity over all nodes was 17.60 lu ts^{-1}; the in/outflow area was 336 × 336 lu^2; and the domain length across which the pressure drop occurred was 336 lu. Thus, the observed Darcy flux was

$$q = \frac{17.60}{336 \times 336} = \frac{k}{\rho(\tau - 0.5)\delta t}\frac{\Delta\rho}{L}$$

$$= \frac{k \times 0.000546}{1 \times (1.0 - 0.5) \times 336}, \qquad (3)$$

which can be rearranged to solve for the intrinsic permeability, $k = 47.93$ lu^2. Conversion of "lu^2" to real permeability units requires multiplication by the scale conversion factor as follows:

$$k_{physical} = k_{LBM}\left(\frac{L_{physical}}{L_{LBM}}\right)^2, \qquad (4)$$

where L is the length of any comparable feature in physical and LBM units. A convenient value is the physical length of a single pixel or lattice

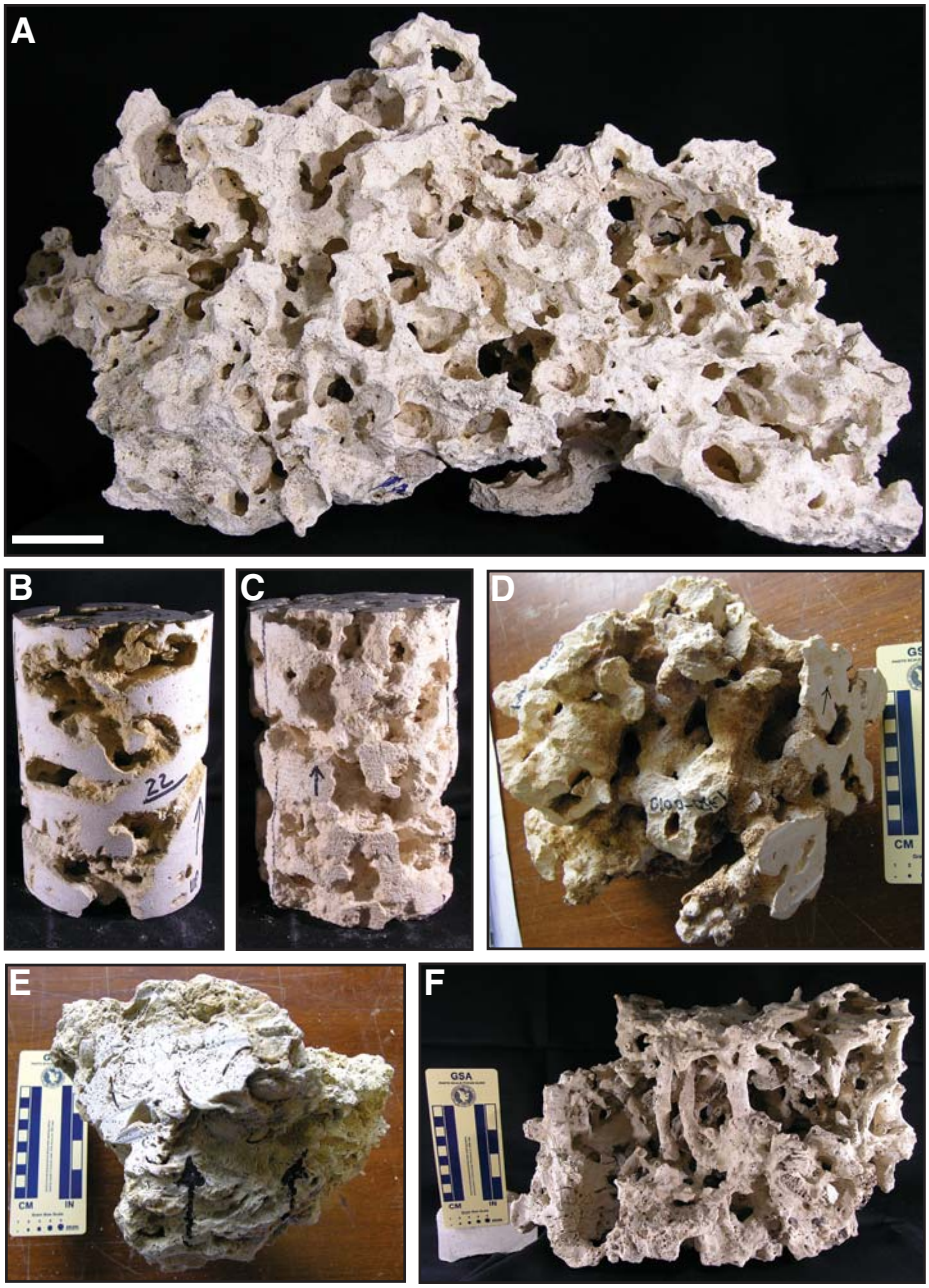

Figure 13. High-resolution X-ray computed tomography scans were conducted on these samples and used to produce volume renderings used in measurements of macroporosity and lattice Boltzmann calculation of intrinsic permeability. (A) High intraburrow macroporosity in a peloid, ooid grain-dominated packstone to grainstone from the high-frequency cycle of the Miami Limestone correlated with marine isotope stage 5e, ML-1. Bar scale = 5 cm. (B) Sandy skeletal wackestone to grain-dominated packstone from a high-frequency cycle of the Fort Thompson Formation assigned to MIS 11, G-3837–22. Intraburrow macroporosity is in *Ophiomorpha*. Diameter of core sample is 10.1 cm. (C) Peloid grainstone from the high-frequency cycle of the Miami Limestone assigned to MIS 5e (G-3837–18) with abundant partly filled *Ophiomorpha*. Diameter of core is 10.1 cm. (D) Peloid, *Halimeda* mud-dominated packstone to grainstone from the high-frequency cycle of the Miami Limestone assigned to MIS 5e, C100-Q5e-1. Mainly interburrow macroporosity. (E) Pelecypod rudstone with matrix of sandy, skeletal packstone. Macroporosity is mostly molds of pelecypod shells. Sample is from lower part of high-frequency cycle 3a of the Fort Thompson Formation, FPL-Q3a-2. (F) Holocene rhizomorphs of mangrove (?) roots (KBM-1) displaying very high interroot macroporosity.

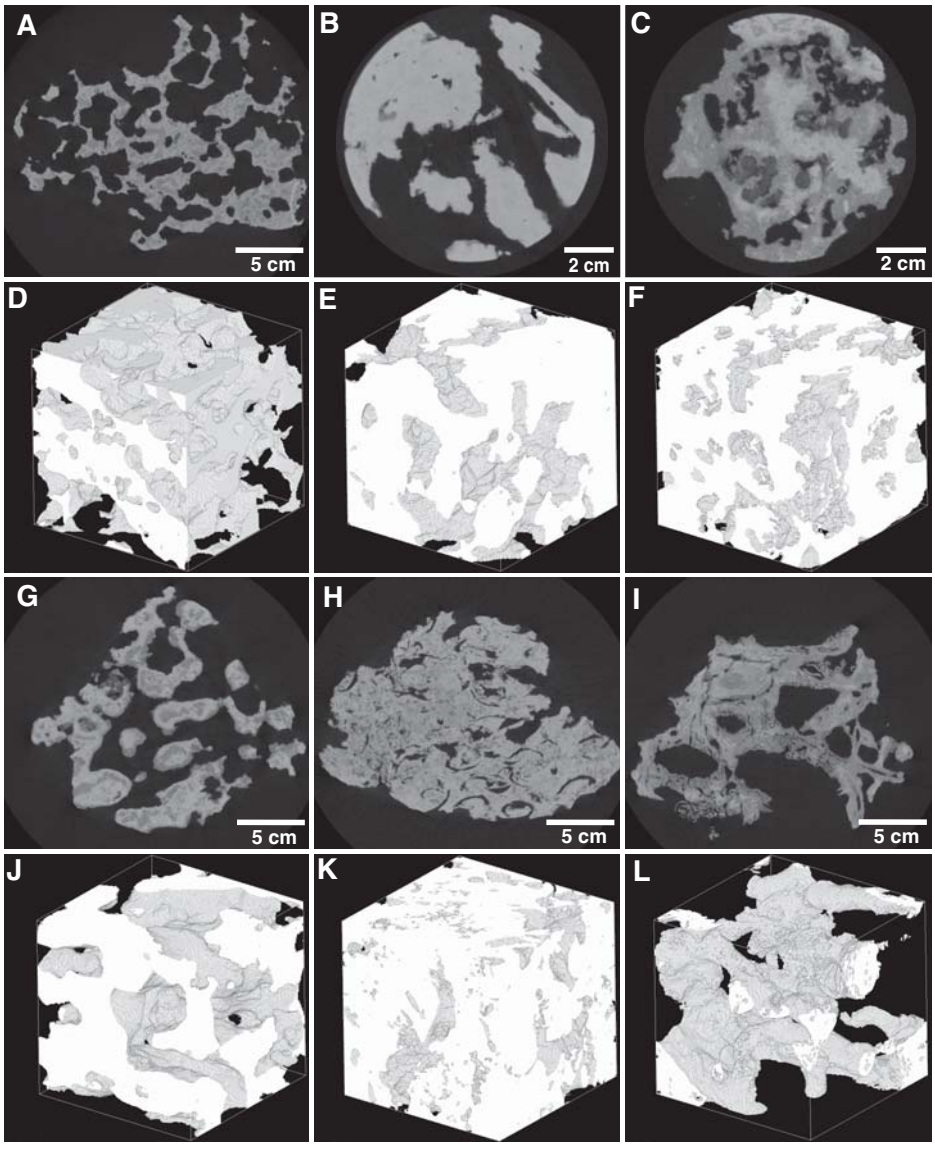

Figure 14. High-resolution X-ray computed tomography scan images and 8.6 cm³ volume renderings used to measure macroporosity and lattice Boltzmann calculation of intrinsic permeability. (A) Scan image of peloid, ooid grain-dominated packstone to grainstone, ML-1. (B) Scan image of sandy skeletal wackestone to grain-dominated packstone, G-3837–22. (C) Scan image of peloid grainstone, G-3837–18. (D) Volume rendering of peloid, ooid grain-dominated packstone to grainstone, ML-1. Calculated macroporosity = 50%; vertical hydraulic conductivity = 34.6 m/s. (E) Volume rendering of sandy skeletal wackestone to grain-dominated packstone, G-3837–22. Calculated macroporosity = 22%; vertical hydraulic conductivity = 1.59 m/s. (F) Volume rendering of peloid grainstone, G-3837–18. Calculated macroporosity = 29%; vertical hydraulic conductivity = 0.298 m/s. (G) Scan image of peloid, *Halimeda* mud-dominated packstone to grainstone, C100-Q5e-1. (H) Scan image of pelecypod rudstone, FPL-Q3a-2. (I) Scan image of mangrove (?) rhizomorphs, KBM-1. (J) Volume rendering of peloid, *Halimeda* mud-dominated packstone to grainstone, C100-Q5e-1. Calculated macroporosity = 64%; vertical hydraulic conductivity = 20.6 m/s. (K) Volume rendering of pelecypod rudstone, FPL-Q3a-2. Calculated macroporosity = 23%; vertical hydraulic conductivity = 0.302 m/s. (L) Volume rendering of mangrove (?) rhizomorphs, KBM-1. Calculated macroporosity = 81%; vertical hydraulic conductivity = 167 m/s.

unit, 0.271 mm/lu in this case. The real intrinsic permeability in this case is 3.52 mm² or 3.52 × 10^{-6} m².

More commonly employed units for intrinsic permeability are millidarcies (mD), where ~1 mD = 10^{-8} m/s. For four of our macroporous samples, we have both LBM-calculated permeability values and laboratory-measured air-permeability values (Table 1). It is interesting to note that LBM-calculated permeability values range from three to five orders of magnitude higher than laboratory measured values (Fig. 15), which are limited for application to extremely permeable macroporous rock samples. An important advantage of using LBM values is the ability to accurately measure permeability in macroporous media. The accuracy of the LBM results has been established based on their close conformance to analytical solutions for flow in pipes and ducts (Alvarez, 2007). LBM calculations offer a new means of obtaining accurate permeability values for macroporous rocks.

The hydraulic conductivity, K, can be obtained from the intrinsic permeability by taking Earth's gravity, g, and the kinematic viscosity of water, ν_{water}, into account, such that $K = kg/\nu_{water}$. In the case of sample ML-1, vertical K = 34.6 m/s (Fig. 14D; Table 1).

The in situ orientations of all samples other than ML-1 were known. The intrinsic permeabilities of the samples were measured in the vertical and horizontal planes and converted to hydraulic conductivity, and these are listed in Table 1. The results indicated relatively minor hydraulic conductivity differences with direction (always less than a factor of 2), and there was no clear dependence of the magnitude of the conductivity on direction. For example, sample C-100-Q5e-1 had a lower horizontal conductivity (12.5 m/s) than vertical conductivity (20.6 m/s), while FPL-Q3a-2 had higher conductivity in the horizontal (0.386 m/s) than in the vertical direction (0.302 m/s).

DISCUSSION

Hydrologic Impacts of Burrow-Related Macroporosity in the Biscayne Aquifer

Our data, combined with established chemical and particulate tracer studies (Renken et al., 2005, 2008; Harvey et al., 2008) within our study area, indicate that zones of burrow-related macroporosity can act as important passageways for advective transport of solutes and pathogens. The widespread nature of callianassid burrowing on shallow-marine carbonate platforms can impart continuity in callianassid-generated ichnofabrics (*Ophiomorpha*) that manifests as

TABLE 1. POROSITY, PERMEABILITY, AND HYDRAULIC CONDUCTIVITY DETERMINED BY COMPUTER METHODS AND LABORATORY ANALYSES

Sample number	Volume of rendering used in LBMs (cm^3)	Macroporosity derived by pixel counting (%)	Laboratory-measured helium porosity (%)	LBM-derived intrinsic permeability (mD)	LBM-derived hydraulic conductivity (m/s)*	Laboratory-measured air permeability (mD)	Hydraulic conductivity calculated from laboratory-measured permeability† (m/s)
KBM-1	29	81	n.d.	1.4×10^{10H}	136^{H}	n.d.	n.d.
				1.7×10^{10V}	167^{V}	n.d.	n.d.
ML-1	28	50	n.d.	1.9×10^{9H}	18.9^{H}	n.d.	n.d.
				3.5×10^{9V}	34.6^{V}	n.d.	n.d.
G-3837-18	10	29	52.2	1.5×10^{7H}	0.148^{H}	4642^{Hmax}	0.00005^{Hmax}
				3.0×10^{7V}	0.298^{V}	$10{,}641^{V}$	0.0001^{V}
C100-Q5e-1	27	64	59.2	1.3×10^{9H}	12.5^{H}	$125{,}341^{H}$	0.001^{H}
				2.1×10^{9V}	20.6^{V}	n.d.	n.d.
FPL-Q3a-1	24	16	n.d.	0^{H}	0^{H}	n.d.	n.d.
				0^{V}	0^{V}	n.d.	n.d.
FPL-Q3a-2	27	23	39.4	3.9×10^{7H}	0.386^{H}	$66{,}058^{H}$	0.0006^{H}
				3.1×10^{7V}	0.302^{V}	n.d.	n.d.
G-3837-22	10	22	32.0	2.2×10^{8H}	2.16^{H}	3178^{Hmax}	0.00003^{Hmax}
				1.6×10^{8V}	1.59^{V}	1332^{V}	0.00001^{V}

Note: The highest range of accurately measured air permeability values is between 10 and 30 Darcies or about 0.0001 m/s and 0.0003 m/s, respectively. LBM—lattice Boltzmann method; H—horizontal permeability or hydraulic conductivity; Hmax—maximum horizontal permeability or hydraulic conductivity; V—vertical permeability or hydraulic conductivity; n.d.—not determined; mD—millidarcy.

*Hydraulic conductivity obtained from LBM intrinsic permeability using $K = kg/v_{water}$, as explained in text.

†Calculated from permeability values using a factor of 1 mD equal to 9.664×10^{-9} m/s.

broadly connected stratiform burrow-related macroporosity. This macroporosity can effectively link areas of aquifer recharge, such as quarried rock mines that are vulnerable to contamination, and discharge points, e.g., municipal well fields. Thus, stratiform zones of burrow-related macroporosity can provide extensive well-connected passageways for the long-distance advective transport to municipal wells (Renken et al., 2005, 2008; Harvey et al., 2008).

To emphasize the extremely high values of our LBM-derived permeabilities (Table 1), we note that they are as much as five orders of magnitude greater than the upper limit of karst limestone permeability shown in Table 2.2 of Freeze and Cherry (1979). Our very high values of permeability for ichnologically influenced macroporous preferential flow zones within the Biscayne aquifer suggest that these zones can accommodate non-Darcian turbulent flow. In our main study area (Fig. 1), Shoemaker et al. (2008) used a dual-porosity modeling technique for the Biscayne aquifer that simulated turbulent groundwater flow under realistic hydraulic gradients within stratiform zones dominated by biogenic macroporosity. These dual-porosity simulations raise questions (Shoemaker et al., 2008) as to the accuracy of equivalent porous media groundwater modeling results in the Biscayne aquifer because these models assume laminar flow in uniformly distributed void spaces and do not adequately define macroporous preferential flow conditions present in the aquifer.

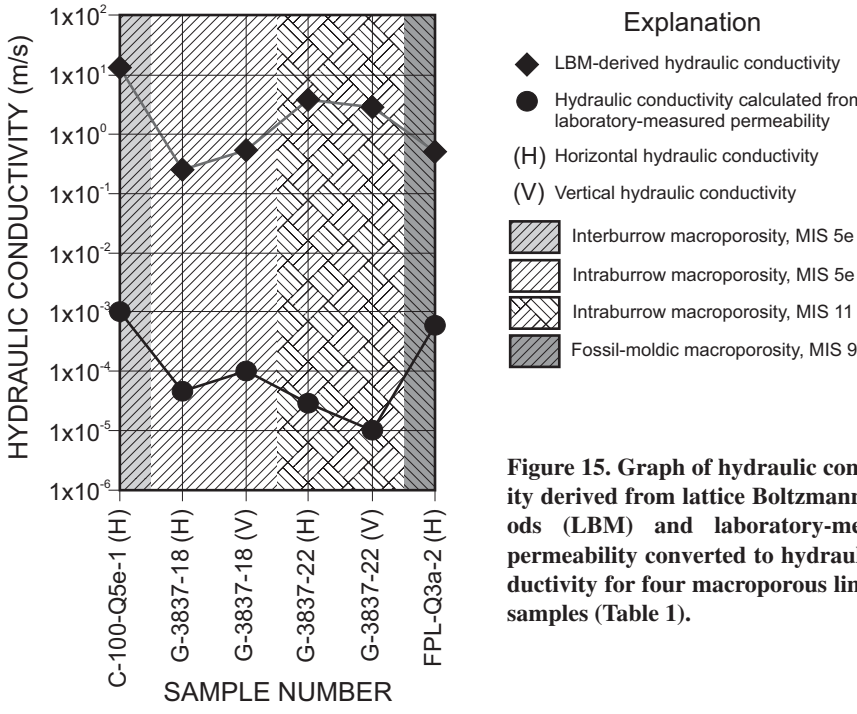

Figure 15. Graph of hydraulic conductivity derived from lattice Boltzmann methods (LBM) and laboratory-measured permeability converted to hydraulic conductivity for four macroporous limestone samples (Table 1).

Examples of *Ophiomorpha* and *Thalassinoides* in Burrow-Related Macroporosity of Carbonate Aquifers

Though macroporosity related to thalassinidean-constructed ichnofabrics is conspicuous and widespread in our study area, it has not been extensively discussed in the context of other carbonate aquifers where it is present, such as in the Cenozoic limestone of the Great Bahama Bank (Beach, 1995) and Cretaceous limestone of the Edwards aquifer (Rose, 1972; Barker and Ardis, 1996). Our data show that an *Ophiomorpha* ichnofabric, created by the burrowing activity of callianassid shrimp, is the major ichnofabric associated with zones of substantial groundwater flow in the Biscayne aquifer. Based on comparative field observations by coauthor Curran, it is suggested that callianassids were the major contributor to the burrow-related macroporosity that Beach (1995, their Figs. 10A, 12B, and 12C) showed to be present in shallow-marine

Quaternary limestone of the Great Bahama Bank. We suggest that macroporosity related to *Ophiomorpha* and other burrows in carbonate aquifers may have been overlooked in some cases, especially in karsted platform carbonates of Middle Jurassic and younger age—the generally accepted age range of *Ophiomorpha* (Häntzschel, 1975). In addition, field work by Cunningham indicates that a stratiform, cycle-bound *Thalassinoides* ichnofabric, likely generated by noncallianassid thalassinidean shrimp (possibly upogebiids), dominates the burrow-related macroporosity reported by Rose (1972) in limestone of the Edwards aquifer.

Comparison between Burrow-Related Eogenetic Porosity in the Biscayne Aquifer and Burrow-Related Mesogenetic or Telogenetic Porosity in Carbonate Reservoirs

Burrow fabrics have economic importance to carbonate hydrocarbon reservoirs within the mesogenetic burial realm because they can result in dense networks of interconnected enhanced porosity and permeability (Flügel, 2004). Our study describes a young, virtually unburied (eogenetic zone of burial) example of burrow-related porosity that provides an opportunity for comparison to older, deep-subsurface burrow-related porosity (mesogenetic zone of burial) in carbonate hydrocarbon reservoirs or their shallow uplifted equivalents that are in the telogenetic zone of burial (e.g., Kendall, 1977; Pu and Qing, 2003; Keswani and Pemberton, 2007). Porosity associated with burrow-related fabrics in carbonate reservoirs or outcrop equivalents is commonly thin-section–scale interparticle or intercrystalline porosity (e.g., Kendall, 1977; Pu and Qing, 2003; Keswani and Pemberton, 2007), where much of any primary intraburrow porosity has been reduced by burrow collapse or filling by sediment or both (Choquette and Pray, 1970).

Using the Ordovician Selkirk Member of the Red River Formation (Gingras et al., 2004; Pemberton and Gingras, 2005) as an example of carbonate rocks in the telogenetic zone of burial, the average burrow permeability of quarried carbonate samples is 19.2 mD, approximately eight orders of magnitude less than our highest value of LBM-derived intraburrow permeability (Table 1). Smith et al. (2003) found that high-permeability skeletal-pelletal grainstone units with interparticle porosity in core contribute to most of the oil production from Cretaceous carbonates at the Al Ghubar field, Oman. They showed that though thin-section–scale interparticle porosity associated with burrow fill is important in terms of overall net porosity thickness, the burrows are not connected well enough to produce substantial volumes of oil. The important point is that the dimensions of the burrow-related pore space of the carbonate reservoir rocks (mesogenetic or telogenetic burial zone) is of the thin-section scale and not the very highly permeable centimeter-scale that is common in burrow-influenced macroporosity of the limestone of the Biscayne aquifer (eogenetic burial stage). In some cases, dissolution of the interburrow matrix of the limestone of the Biscayne aquifer has expanded porosity to the cavernous scale (Cunningham et al., 2008).

Comparison between the Permeabilities of Biscayne Aquifer Biogenic Macroporosity and "Super-K" Zones in Ghawar Field

The world's largest, most prolific oil field is the Ghawar field, Saudi Arabia, which produces primarily from the Arab-D carbonate reservoir within the Upper Jurassic Arab and Jubaila Formations. Much of the production is from grain-dominated limestone, but a substantial contribution originates from very high permeability stratiform flow zones. The term "super-K" has been attributed to these zones, which have characteristically extremely high flow and are defined as having production greater than 500 barrels per day per foot of vertical interval (Meyer et al., 2000). Super-K zones are interpreted to occur where dolomitized facies containing molds of stromatoporoids (especially *Cladocoropsis*) form thin layers of very effective touching-vug porosity (Lindsay et al., 2006). Alternatively, Pemberton and Gingras (2005) proposed that the super-K flow zones are primarily associated with ichnofabrics. They report that stratiform super-K flow zones are related to burrow-enhanced permeability represented by firm-ground *Thalassinoides* systems filled with detrital sucrosic dolomite, thus forming a biogenic flow system.

The permeability of the Ghawar super-K flow zones ranges between 1 and 530 Darcies (Schon and Head, 2007, their Table 1). The highest reported Ghawar permeability is thus two to five orders of magnitude less than the Biscayne aquifer permeabilities derived by LBMs applied to samples with biogenic macroporosity (Table 1). Also, the Arab-D wells have the ability to produce up to 4×10^4 bbl/d (~6.4×10^6 L/d), where bbl is barrel, as compared to ~4.1×10^7 L/d pumped from a municipal Biscayne aquifer water-supply well (S-3164) effectively connected to zones of burrow-related macroporosity (Renken et al., 2005; Cunningham et al., 2006a; Schon and Head, 2007). The comparisons between permeability and production suggest that certain biogenic flow units of the Biscayne aquifer have more extreme permeabilities than the super-K zones at the Ghawar field.

SUMMARY AND CONCLUSIONS

In our main study area, much of the groundwater flow in the Biscayne aquifer is related to biogenic touching-vug macroporosity, which forms tabular-shaped stratiform groundwater flow zones. The biogenic macroporosity is largely manifested as: (1) ichnogenic macroporosity related to postdepositional burrowing activity, primarily by callianassid shrimp; and (2) biomoldic macroporosity formed by dissolution of organism hard parts, principally mollusk shells. Although vertical solution pipes, bedding plane and irregular vugs, and matrix porosity certainly play a role in groundwater movement, this is the first time that biogenic macroporosity has been fully characterized in terms of its physical and hydraulic nature within a karst carbonate aquifer. As such, we provide a detailed view of several types of biogenic macroporosities that have received little attention in research on karst carbonate aquifers, especially the very prominent callianassid-related macroporosity.

The hydrologic importance of biogenic porosity in the Biscayne aquifer was evaluated for the study area by combining analyses of cyclostratigraphy, ichnology, and borehole-geophysical analyses of core holes; tracer-test analyses; and lattice-Boltzmann flow simulations. Results show that stratiform tabular-shaped units of thalassinidean-associated macroporosity are commonly confined to the lower part of upward-shallowing high-frequency cycles, throughout aggradational high-frequency cycles, and, in one case, stack vertically within the lower part of an upward-shallowing progradational high-frequency cycle set. Thus, *Ophiomorpha* ichnofabric and related macroporosity are commonly found in the lower part of upward-shallowing cyclicity at two scales, and greatest concentrations of this macroporosity occur in that general part of the high-frequency cycles and the high-frequency cycle set where the deepest paleodepth is interpreted.

Borehole–flow meter, fluid-conductivity, fluid-temperature, and digital borehole image data across 64 flow zones in 16 boreholes indicate that biogenic porosity is the principal pore type in groundwater flow zones, and ichnogenic macroporosity is important in most. Bedding-plane vugs or irregular vugs were found to be a subordinate contribution to flow zones, and only a single cavernous-sized flow zone was identified. However, outside our main study area, such as at Deering Glade, the presence of cavernous porosity, and its association with *Ophiomorpha*-related macroporosity within the part of the Miami Limestone correlated to MIS 5e, is notable. To emphasize the importance of

the potential for *Ophiomorpha*-related macroporosity to control groundwater flow, ~77% of the vertical thickness (~12 net m) of the Biscayne aquifer is characterized by this pore type in one borehole (G-3849) on the western perimeter of the main study area. Since callianassids are widespread, prolific endolithic burrowers of tropical, shallow-marine carbonate sediment, there can be broad continuity of macroporosity associated with *Ophiomorpha* ichnofabrics, thus making the aquifer vulnerable to long-distance transport of contaminants via this well-connected macropore type.

Three-dimensional CT renderings of macroporous limestone samples indicate that complex flow paths exist within the tightly spaced burrow complexes. When combined with LBM flow modeling, CT data allowed us to quantify the range in permeability of various types of Biscayne aquifer biogenic macroporosity. The results were consistent with field observations. We showed for the first time that ichnofabric-related porosity is likely the major control on permeability in the Biscayne aquifer within the main study area, and possibly in other carbonate aquifers affected by eogenetic karst as well.

LBMs are capable of quantifying the permeability of highly macroporous samples, such as those that control groundwater flow in the Biscayne aquifer. Standard laboratory techniques may not be able to accomplish this, and physical measurements are fraught with difficulties. The extreme permeabilities (as high as 3.5×10^6 Darcies or 34.6 m/s hydraulic conductivity) associated with burrow-related macroporosity in the Biscayne aquifer suggest that non-Darcian turbulent flow is possible within widespread zones characterized by this pore type, even at very low hydraulic gradients.

We suggest that the stratiform ichnogenic groundwater flow zones of the Biscayne aquifer are superpermeability flow zones and are even more extreme (~2–5 orders of magnitude higher) than the "super-K" zones of the world's largest oil field (Ghawar field, Saudi Arabia). Thus, the ichnogenic flow zones of the Biscayne aquifer provide tremendous examples for future comparative studies on the origin and progressive reduction of burrow-related macroporosity in reservoirs and carbonate aquifers as macroporosity evolves from eogenetic to telogenetic burial zones.

ACKNOWLEDGMENTS

The National Science Foundation (grant 0440253) helped fund Huang and Sukop. The Priority Ecosystems Science (U.S. Geological Survey) and Critical Ecosystems Studies Initiative (Everglades National Park) programs provided major project funding and additional support to Florida International University coauthors. Mike Wacker assisted with data acquisition. Reviews by A.A. "Tony" Ekdale, Valleta Watson, Stephen Worthington, Duncan McIlroy, and Brian Pratt greatly improved the paper.

REFERENCES CITED

Alvarez, P.F., 2007, Lattice Boltzmann modeling of fluid flow to determine the permeability of a karst specimen [M.S. thesis]: Miami, Florida International University, 96 p.

Barker, R.A., and Ardis, A.F., 1996, Hydrogeologic framework of the Edwards-Trinity aquifer system, west-central Texas: U.S. Geological Survey Professional Paper 1421-B, 61 p.

Beach, D.K., 1995, Controls and effects of subaerial exposure on cementation and development of secondary porosity in the subsurface of Great Bahama Bank, *in* Budd, D.A., Saller, A.H., and Harris, P.M., eds., Unconformities and Porosity in Carbonate Strata: American Association of Petroleum Geologists Memoir 63, p. 1–33.

Choquette, P.W., and Pray, L.C., 1970, Geologic nomenclature and classification of porosity in sedimentary carbonates: American Association of Petroleum Geologists Bulletin, v. 54, p. 207–250.

Collins, R.E., 1952, Determination of the transverse permeabilities of large core samples from petroleum reservoirs: Journal de Physique, v. 23, p. 681–684.

Cressler, A., 1993, The caves of Dade County, Florida, *in* Georgia Underground: Dogwood City Grotto: National Speleological Society, v. 30, no. 3, p. 9–16.

Cunningham, K.J., Carlson, J.I., and Hurley, N.F., 2004a, New method for quantification of vuggy porosity from digital optical borehole images as applied to the karstic Pleistocene limestone of the Biscayne aquifer, southeastern Florida: Journal of Applied Geophysics, v. 55, p. 77–90, doi: 10.1016/j.jappgeo.2003.06.006.

Cunningham, K.J., Carlson, J.L., Wingard, G.L., Robinson, E., and Wacker, M.A., 2004b, Characterization of aquifer heterogeneity using cyclostratigraphy and geophysical methods in the upper part of the karstic Biscayne aquifer, southeastern Florida: U.S. Geological Survey Water-Resources Investigation Report 03–4208, 46 p.

Cunningham, K.J., Renken, R.A., Wacker, M.A., Zygnerski, M.R., Robinson, E., Shapiro, A.M., and Wingard, G.L., 2006a, Application of carbonate cyclostratigraphy and borehole geophysics to delineate porosity and preferential flow in the karst limestone of the Biscayne aquifer, SE Florida, *in* Harmon, R.S., and Wicks, C., eds., Perspectives on Karst Geomorphology, Hydrology, and Geochemistry—A Tribute Volume to Derek C. Ford and William B. White: Geological Society of America Special Paper 404, p. 191–208, doi:10.1130/2006.2404(16).

Cunningham, K.J., Wacker, M.A., Robinson, E., Dixon, J.F., and Wingard, G.L., 2006b, A cyclostratigraphic and borehole geophysical approach to development of a three-dimensional conceptual hydrogeologic model of the karstic Biscayne aquifer, southeastern Florida: U.S. Geological Survey Scientific Investigations Report 2005–5235, 69 p.

Cunningham, K.J., Sukop, M.C., Huang, H., Alvarez, P.F., Curran, H.A., Wacker, M.A., Florea, L.J., Renken, R.A., and Dixon, J.F., 2008, Biogenic macroporosity and its lattice Boltzmann method permeability in the karst Biscayne aquifer, *in* Sasowsky, I.D., Feazel, C.T., Mylroie, J.E., Palmer, A.N., and Palmer, M.V., eds., Karst from Recent to Reservoirs: Special Publication 14: Leesburg, Virginia, Karst Waters Institute (in press).

Curran, H.A., 2007, Ichnofacies, ichnocoenoses, and ichnofabrics of Quaternary shallow-marine to dunal tropical carbonates: A model and implications, *in* Miller, W., III, ed., Trace Fossils: Concepts, Problems, Prospects: Amsterdam, Elsevier, p. 232–247.

Curran, H.A., and Martin, A.J., 2003, Complex decapod burrows and ecological relationships in modern and Pleistocene intertidal carbonate environments, San Salvador Island, Bahamas: Palaeogeography, Palaeoclimatology, Palaeoecology, v. 192, p. 229–245, doi: 10.1016/S0031-0182(02)00687-9.

Evans, C.C., 1984, Development of an ooid sand shoal complex: The importance of antecedent and syndepositional topography, *in* Harris, P.H., ed., Carbonate Sands—A Core Workshop: Society of Economic Paleontologists Mineralogists Core Workshop No. 5, p. 392–428.

Evans, C.C., and Ginsburg, R.N., 1987, Fabric-selected diagenesis in the late Pleistocene Miami Limestone: Journal of Sedimentary Petrology, v. 57, p. 311–318.

Fish, J.E., and Stewart, M., 1991, Hydrogeology of the surficial aquifer system, Dade County, Florida: U.S. Geological Survey Water-Resources Investigations Report 80–4108, 50 p., 11 pls.

Flügel, E., 2004, Microfacies of Carbonate Rocks: Berlin, Springer, 976 p.

Ford, D.C., and Williams, P.W., 1989, Karst Geomorphology and Hydrogeology: London, Unwin Hyman, 601 p.

Freeze, R.A., and Cherry, J.A., 1979, Groundwater: Englewood Cliffs, New Jersey, Prentice-Hall, 604 p.

Galli, G., 1991, Mangrove-generated structures and depositional model of the Pleistocene Fort Thompson Formation (Florida Plateau): Facies, v. 25, p. 297–314, doi: 10.1007/BF02536763.

Gingras, M.K., Mendoza, C.A., and Pemberton, S.G., 2004, Fossilized worm burrows influence the resource quality of porous media: American Association of Petroleum Geologists Bulletin, v. 88, p. 875–883.

Halley, R.B., and Evans, C.C., 1983, The Miami Limestone: A Guide to Selected Outcrops and Their Interpretation: Miami, Florida, Miami Geological Society, 67 p.

Halley, R.B., Shinn, E.A., Hudson, J.H., and Lidz, B.H., 1977, Pleistocene barrier bar seaward of ooid shoal complex near Miami, Florida: The American Association of Petroleum Geologists Bulletin, v. 61, p. 519–526.

Häntzschel, W., 1975, Trace fossils and problematica, *in* Teichert, C., ed., Treatise on Invertebrate Paleontology: Part W. Miscellanea, Supplement 1, Trace Fossils and Problematica (2nd edition): Boulder, Colorado and Lawrence, Kansas, Geological Society of America and University of Kansas, 269 p.

Harris, J.G., Mylroie, J.E., and Carew, J.L., 1995, Banana holes: Unique karst features of the Bahamas: Carbonates and Evaporites, v. 10, p. 215–224.

Harvey, R.W., Metge, D.W., Shapiro, A.M., Renken, R.A., Osborn, C.L., Ryan, J.N., Cunningham, K.J., and Landkamer, L., 2008, Assessing vulnerability of a southeast Florida municipal well field. 3. Use of microspheres to estimate the transport potential of *Cryptosporidium parvum* oocysts in karstic limestone of the Biscayne aquifer: Water Resources Research (in press).

Kendall, A.C., 1977, Origin of dolomite mottling in Ordovician limestones from Saskatchewan and Manitoba: Bulletin of Canadian Petroleum Geology, v. 25, p. 480–503.

Keswani, A.D., and Pemberton, S.G., 2007, Applications of ichnology in exploration and exploitation of Mississippian carbonate reservoirs, Midale Beds, Weyburn Oilfield, Saskatchewan: Calgary, Alberta, Canada, Canadian Society of Petroleum Geologists and Canadian Society of Exploration Geophysicists Conference, 14–17 May 2007, Extended Abstract, 28 p.

Ketcham, R.A., and Carlson, W.D., 2001, Acquisition, optimization and interpretation of X-ray computed imagery: Applications to geosciences: Computers & Geosciences, v. 27, p. 381–400, doi: 10.1016/S0098-3004(00)00116-3.

Lindsay, R.F., Cantrell, D.L., Hughes, G.W., Keith, T.H., Mueller, H.W., III, and Russell, S.D., 2006, Ghawar Arab-D reservoir: Widespread porosity in shoaling-upward carbonate cycles, Saudi Arabia, *in* Harris, PM., and Weber, L.J., eds., Giant Hydrocarbon Reservoirs of the World: From Rocks to Reservoir Characterization and Modeling: American Association of Petroleum Geologists Memoir 88, p. 97–137.

Lucia, F.J., 1995, Rock fabric/petrophysical classification of carbonate pore space for reservoir characterization: The American Association of Petroleum Geologists Bulletin, v. 79, p. 1275–1300.

Meyer, F.O., Price, R.C., and Al-Raini, S.M., 2000, Stratigraphic and petrophysical characteristics of cored Arab-D Super-k intervals, Hawiyah Area, Ghawar field, Saudi Arabia: GeoArabia, v. 5, p. 355–384.

Multer, H.G., Gischler, E., Lundberg, J., Simmons, K.R., and Shinn, E.A., 2002, Key Largo Limestone revisited: Pleistocene shelf-edge facies, Florida Keys, USA: Facies, v. 46, p. 229–272, doi: 10.1007/BF02668083.

Parker, G.G., et al., 1955, Water resources of southeastern Florida: U.S. Geological Survey Water-Supply Paper 1255, 965 p.

Pemberton, S.G., and Gingras, M.K., 2005, Classification and characterization of biogenically enhanced hydraulic conductivity: American Association of Petroleum Geologists Bulletin, v. 89, p. 1493–1517.

Perkins, R.D., 1977, Depositional framework of Pleistocene rocks in south Florida, *in* Enos, P., and Perkins, R.D., eds., Quaternary Sedimentation in South Florida: Geological Society of America Memoir 147, p. 131–198.

Pu, R., and Qing, H., 2003, Pool characterization of Ordovician Midale Field: Implications for Red River play in northern Williston Basin, southeastern Saskatchewan, Canada: American Association of Petroleum Geologists Bulletin, v. 87, p. 1699–1715.

Renken, R.A., Shapiro, A.M., Cunningham, K.J., Harvey, R.W., Metge, D.W., Zygnerski, M.R., Osborn, C.L., Wacker, M.A., and Ryan, J.N., 2005, Assessing the vulnerability of a municipal well field to contamination in a karst aquifer: Environmental & Engineering Geoscience, v. 11, p. 341–354.

Renken, R.A., Cunningham, K.J., Shapiro, A.M., Harvey, R.W., Zygnerski, M.R., Metge, D.W., and Wacker, M.A., 2008, Chemical and pathogen transport in the karstic limestone of the Biscayne aquifer: 1. Revised conceptualization of groundwater flow: Water-Resources Research (in press).

Rose, P.R., 1972, Edwards Group, surface and subsurface, Central Texas: The University of Texas at Austin, Bureau of Economic Geology Report of Investigations No. 74, 198 p.

Schon, S.C., and Head, J.W., 2007, Super-permeability zones and the formation of outflow channels on Mars: League City, Texas, 38th Lunar and Planetary Science Conference: http://www.lpi.usra.edu/meetings/lpsc2007/pdf/2135.pdf (May 2008).

Shinn, E.A., 1968, Burrowing in recent lime sediments of Florida and the Bahamas: Journal of Paleontology, v. 42, p. 879–894.

Shoemaker, W.B., Cunningham, K.J., Kuniansky, E.L., and Dixon, J., 2008, Effects of turbulence on hydraulic heads and parameter sensitivities in preferential groundwater flow layers: Water Resources Research, v. 44, W03501, doi: 10.1029/2007WR006601.

Smith, L.B., Eberli, G.P., Masaferro, J.L., and Al-Dhahab, S., 2003, Discrimination of effective from ineffective porosity in heterogeneous Cretaceous carbonates, Al Ghubar field, Oman: The American Association of Petroleum Geologists Bulletin, v. 87, p. 1509–1529.

Succi, S., 2001, The Lattice Boltzmann Equation for Fluid Dynamics and Beyond: Oxford, Clarendon Press, 288 p.

Sukop, M.C., and Thorne, D.T., Jr., 2006, Lattice Boltzmann Modeling: An Introduction for Geoscientists and Engineers: New York, Springer, 172 p.

Tedesco, L.P., and Wanless, H.R., 1991, Generation of sedimentary fabrics and facies by repetitive excavation and storm infilling of burrow networks, Holocene of South Florida and Caicos Platform: B.W.I.: Palaios, v. 6, p. 326–343, doi: 10.2307/3514912.

Vacher, H.L., and Mylroie, J.E., 2002, Eogenetic karst from the perspective of an equivalent porous medium: Carbonates and Evaporites, v. 17, p. 182–196.

Whitaker, F.F., and Smart, P.L., 2000, Characterising scale-dependence of hydraulic conductivity in carbonates: Evidence from the Bahamas: Journal of Geochemical Exploration, v. 69–70, p. 133–137, doi: 10.1016/S0375-6742(00)00016-9.

White, W.B., 1988, Geomorphology and Hydrology of Karst Terrains: New York, Oxford University Press, 464 p.

White, W.B., 1999, Conceptual models for karstic aquifers, *in* Palmer, A.N., Palmer, M.V., and Sasowsky, I.D., eds., Proceedings, 5th Symposium of The Karst Waters Institute: Charlottesville, Virginia, The Karst Waters Institute, p. 11–16.

Worthington, S.R.H., Ford, D.C., and Davies, G.J., 2000, Matrix, fracture and channel components of storage and flow in a Paleozoic limestone aquifer, *in* Sasowsky, I.D., and Wicks, C.M., eds., Groundwater Flow and Contaminant Transport in Carbonate Aquifers: Rotterdam, Balkema, p. 113–128.

Zou, Q., and He, X., 1997, On pressure and velocity boundary conditions for the lattice Boltzmann BGK model: Physics of Fluids, v. 9, p. 1591–1598, doi: 10.1063/1.869307.

Manuscript Received 20 December 2007
Revised Manuscript Received 16 April 2008
Manuscript Accepted 17 April 2008

Printed in the USA